Calibration of groundwater seepage on the spatial distribution of the stream network to assess catchment-scale hydraulic properties

Ronan Abhervé[1], Clément Roques[1,2], Alexandre Gauvain[1,4], Laurent Longuevergne[1], Stéphane Louaisil[3], Luc Aquilina[1], Jean-Raynald de Dreuzy[1]

[1] Univ Rennes, CNRS, Geosciences Rennes – UMR 6118, F-35000 Rennes, France
[2] Centre for Hydrology and Geothermics (CHYN), Université de Neuchâtel, Neuchâtel, Switzerland
[3] Eau du Bassin Rennais, Rennes, France
[4] Laboratoire de Météorologie Dynamique – IPSL, CNRS, Sorbonne Université, 75005 Paris, France

Correspondence to: Ronan Abhervé (ronan.abherve@univ-rennes1.fr, ronan.abherve@gmail.com)

Abstract

The assessment of effective hydraulic properties at the catchment scale, i.e. hydraulic conductivity (K) and transmissivity (T), is particularly challenging due to the sparse availability of hydrological monitoring systems through stream gauges and boreholes. To overcome this challenge, we propose a calibration methodology which only considers information from the digital elevation model (DEM) and the spatial distribution of the stream network. The methodology is built on the assumption that the groundwater system is the main driver controlling the stream density and extension, where the perennial stream network reflects the intersection of the groundwater table with the topography. Indeed, the groundwater seepage at the surface is primarily controlled by the topography, the aquifer thickness, and the dimensionless parameter K/R, where R is the average recharge rate. Here, we use a process-based and parsimonious 3D groundwater flow model to calibrate K/R by minimizing the relative distances between the observed and the simulated stream network generated from groundwater seepage zones. By deploying the methodology on 24 selected headwater catchments located in north-western France, we demonstrate that the method successfully predicts the stream network extent for 80 % of the cases. Results show a high sensitivity of K/R to the extension of the low-order streams and limited impacts of the DEM resolution as long the DEM remains consistent with the stream network observations. By assuming an average recharge rate, we found effective K values to vary between 1.0×10^{-5} and 1.1×10^{-4} m s^{-1} in agreement with local estimates derived from hydraulic tests and independent calibrated groundwater model. With the emergence of global remote-sensing databases compiling information of high-resolution DEM and stream network, this approach provides new opportunities to assess hydraulic properties of unconfined aquifers in ungauged basins.

1 Introduction

Evaluating the availability of water resources and its evolution under global changes requires quantitative assessment of water fluxes at the catchment scale (Fan et al., 2019). Such evaluation involves the development of advanced hydrological models resolving relevant hillslope to catchment-scale processes (Refsgaard et al., 2010; Holman et al., 2012; Wada et al., 2010) in a wide variety of high-stake areas (Elshall et al., 2020; Vergnes et al., 2020). Within the local hydrological cycle, aquifers ensure the storage of water during and after recharge periods, increasing the availability of the resources (Fan, 2015; Fan et al., 2015), and transfer this water to surface systems during rain-free periods (Winter, 1999; Sophocleous, 2002; Alley et al., 2002; Anderson et al., 2015). Quantifying groundwater fluxes remains a challenge, as the hydraulic properties of aquifers, i.e. hydraulic conductivity (K) and transmissivity (T), have classically been constrained through sparse borehole-scale characterization (Anderson et al., 2015; Carrera et al., 2005). They are classically estimated using hydraulic tests at centimeter scales for laboratory experiments up to decameter scales for well tests (Renard, 2005; Freeze and Cherry, 1979; Domenico and Schwartz, 1990). Other methods have been proposed at larger scales based on the analysis of streamflow dynamic (Troch et al., 2013; Mendoza et al., 2003; Vannier et al., 2014; Brutsaert and Nieber, 1977), earth tides (Hsieh et al., 1987; Rotzoll and El-Kadi, 2008) and borehole head dynamics (Zlotnik and Zurbuchen, 2003; Jiménez-Martínez et al., 2013), as well as from the calibration of large scale hydrological models (Eckhardt and Ulbrich, 2003; Etter et al., 2020; Chow et al., 2016). Multi-objective calibration has been proposed to reduce uncertainties, considering complementary data like temperature (Bravo et al., 2002), groundwater ages derived from environmental tracers (Kolbe et al., 2016) or continuous geochemical monitoring (Schilling et al., 2019). In addition, recent advances in machine learning technics show promising results to evaluate hydraulic properties at the regional scale (Cromwell et al., 2021; Marçais and de Dreuzy, 2017; Reichstein et al., 2019).

To tackle the numerous challenges related to the upscaling of hydraulic properties from the local to the regional or global scales, several databases provides exhaustive compilations of measurements performed all around the world (Comunian and Renard, 2009; Achtziger-Zupančič et al., 2017; Ranjram et al., 2015; Kuang and Jiao, 2014). By compiling values obtained from calibrated groundwater models, Gleeson et al. (2014) proposed a global-scale hydraulic conductivity map GLHYMPS, with an update by Huscroft et al. (2018), where values have been interpolated based on a high-resolution global lithology map (GLiM) (Hartmann and Moosdorf, 2012). Besides inconsistencies and methodological biases supported in Gleeson et al. (2014), the compiled permeabilities above the regional scale (>5 km) are not suitable at the catchment scale. Therefore, estimating subsurface hydraulic properties that correctly represent observed catchment-scale processes remains a major challenge for the hydrological community (Blöschl et al., 2019). New opportunities has been identified through the increasing availabilities of surface observations (Beven et al., 2020; Gleeson et al., 2021), specifically with application for ungauged basins.

Information on the spatial distribution of groundwater seepage appears to be a critical observation to use for the calibration of subsurface hydraulic properties in hydrologic models (Grayson and Blöschl, 2000). This approach can be applied under the assumption that the density and extent of the stream network is primarily controlled by groundwater flow. This assumption is

valid under temperate and wet climates, for unconfined aquifers, where surface and subsurface hydrological systems are well connected (Cuthbert et al., 2019; Fan et al., 2013) with important discharge of the aquifer directly into the streams (Haitjema and Mitchell-Bruker, 2005). Indeed, a groundwater seepage network dominantly controls the structure of a continuous stream network, its spatial extent and its ramification (Vries, 1994; Devauchelle et al., 2012; Strahler, 1964; Leibowitz et al., 2018; Pederson, 2001). Under steady state conditions, the distribution of groundwater seepage is then controlled by the characteristic hillslope geometry, the recharge rate (R), and the aquifer transmissivity (T), i.e. the product of the hydraulic conductivity (K) and the saturated aquifer thickness (d_{sat}) (Litwin et al., 2022; Luijendijk, 2021; Bresciani et al., 2014; Haitjema and Mitchell-Bruker, 2005; Gleeson and Manning, 2008). At a given recharge rate, low transmissive aquifers display high groundwater table elevations and, consequently, dense stream networks in the upper part of the catchments. Conversely, highly transmissive aquifers will display lower groundwater tables, higher discharge rates in fewer seepage areas, and, consequently, sparser stream networks confined in the lower elevation valleys (Day, 1980; Lovill et al., 2018; Dunne, 1975; Luo et al., 2016; Dietrich and Dunne, 1993; Godsey and Kirchner, 2014; Prancevic and Kirchner, 2019).

Previous studies have focused on the comparison of an observed hydrographic network with a simulated hydrographic network computed from different methods. The organization of stream networks has been predicted directly from a digital elevation model (DEM) based on a predefined accumulation threshold value determining whether an upstream surface is capable of producing significant flow (Mardhel et al., 2021; Le Moine, 2008; Schneider et al., 2017; Luo and Stepinski, 2008; Lehner et al., 2013). Lumped parameter models, such as TOPMODEL (Beven and Kirkby, 1979), have also been extensively used to predict the spatial patterns of seepage areas (Merot et al., 2003) allowing to constrain the subsurface hydraulic properties (Blazkova et al., 2002; Güntner et al., 2004; Franks et al., 1998). (Luo et al., 2010) proposes a method leading to a spatial distribution of hydraulic conductivities by constraining a 1D groundwater model based on Dupuit-Forcheimer (DF) assumption on drainage dissection patterns. However, these approaches are limited to consider a subsurface flowpath equal and parallel to the downslope topography (Luo and Stepinski, 2008). Relying on explicit simulations of the spatial stream network with a process-based hillslope model following the DF assumption (Weiler and McDonnell, 2004), Stoll and Weiler (2010) proposes to overcome limitation by routing the downslope subsurface flow from the groundwater table by a grid cell by grid cell approach (Wigmosta and Lettenmaier, 1999). The assessed subsurface hydraulic properties are intended to guide the calibration of hydrological models in ungauged basins, only using only a DEM and a hydrographic network map. These approaches are especially relevant as rapid advances in remote sensing are improving the description of global river networks (Schneider et al., 2017; Lehner and Grill, 2013), wetlands (Tootchi et al., 2019; Rapinel et al., 2023) or soil moisture (Vergopolan et al., 2021). Lidar and high-resolution satellite imagery offers new opportunities to determine the surface characteristics of landscapes (Levizzani and Cattani, 2019; Blöschl et al., 2019) and, by extension, the hydrological parameters of local to continental ungauged catchments (Barclay et al., 2020; Dembélé et al., 2020).

In this work, we propose a new methodology to quantify effective hydraulic properties of unconfined aquifers from topographical and stream network observations now available at high resolution. From a parsimonious 3D groundwater flow

model, we aim at estimating the catchment-scale K, based on surface information only, the spatial distribution of the stream network. We propose a novel performance criterion to assess the similarity between the simulated seepage areas and the observed stream network, coupled with a stand-alone calibration procedure. We present the full methodology and its sensitivity to different hydrographic network observation products on 24 catchments covering various geological contexts in north-western France. We finally discuss opportunities and perspectives to systematically characterize aquifers in ungauged catchments from surface observations.

2   Materials and Methods

An overview of the method workflow is illustrated in Figure 1. Each block refers to a specific sub-section detailed below (from 2.1 to 2.5).

1. A digital elevation method (DEM) is used as the top boundary of the groundwater flow model (section 2.2.1);
2. 3D groundwater flow is solved in the model domain and simulated seepage areas are extracted (section 2.2.2);
3. A selected stream network independent of the DEM is taken as the observed reference (section 2.2.3);
4. The dimensionless ratio K/R [-] is calibrated to reach the best match between the simulated seepage areas and the extent of the observed stream network (section 2.2.4);
5. From the optimized K/R, the optimal hydraulic conductivity K_{optim} [L T^{-1}] is deduced by considering the recharge R. The optimal transmissivity T_{optim} [L^2 T^{-1}] is obtained considering the average thickness of the saturated aquifer d_{sat} [L]computed by the model (section 2.2.5).

2.1   Definition of the model domain based on the analysis of the topography

We first select the digital elevation model (DEM) that will be defined as the upper boundary of the groundwater model. In this study, we use the 75 m grid resolution DEM available at the scale of France. It is generated from photogrammetric restitution and provided by BD ALTI (IGN, 2021). We also explore the impact of different DEM resolutions on the final estimations of K/R. We consider two higher resolution DEMs of 5 m and 25 m also provided by BD ALTI. For coarser resolutions, the 25 m DEM was downsampled with nearest neighbour option to larger cell sizes, i.e. 100 m, 200 m, and 300 m.

Geospatial processing is performed using the software WhiteBoxTools available in Python (Lindsay, 2016), labelled *WBT* with the respective functions quoted in brackets in the following. First, the raw DEM is corrected by filling all depressions and by removing flat areas (*WBT.FillDepressions*) to ensure continuous flow between grid cells. The vector point shapefile of the outlet is moved to the location coincident with the highest flow accumulation value (*WBT.D8FlowAccumulation*) within a specified maximum distance taken as twice the DEM resolution (e.g. 150 m for a 75 m resolution DEM) (*WBT.SnapPourPoints*). A flow direction raster (*WBT.D8Pointer*) is used to extract the drainage basin (*WBT.Watershed*).
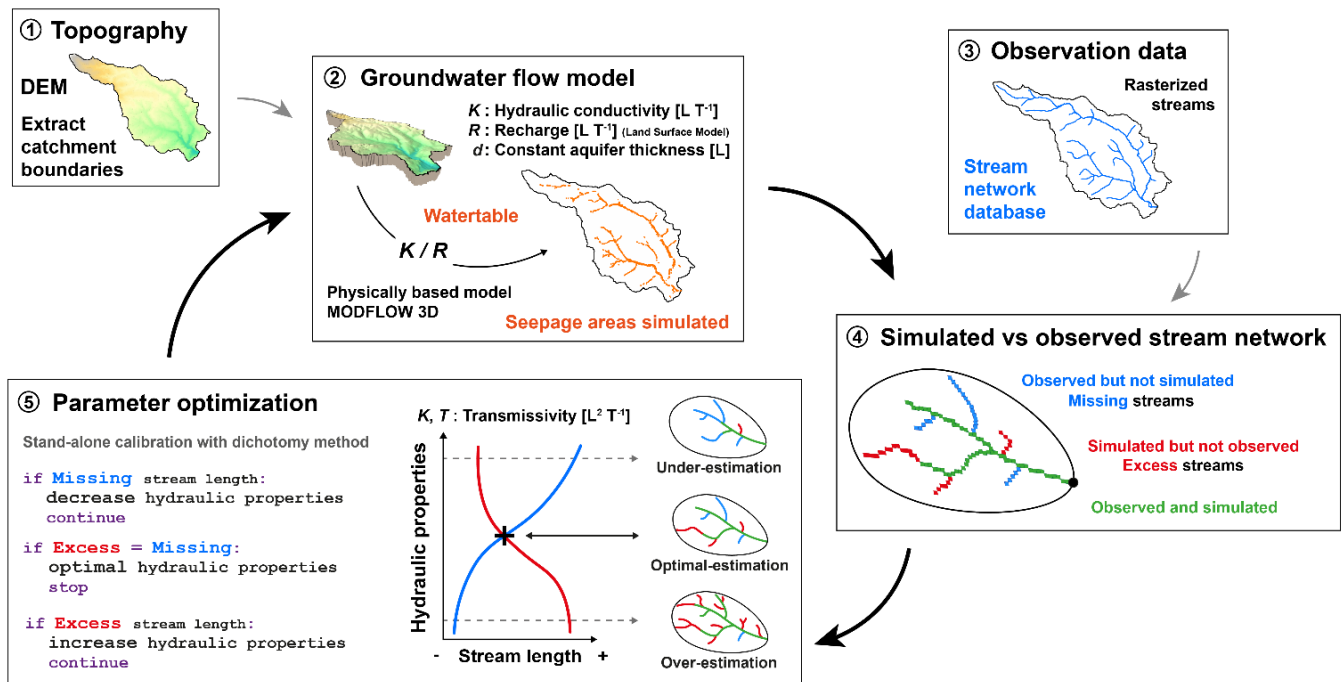
Figure 1. Model workflow for the calibration of subsurface hydraulic properties from observed stream network.

2.2 Groundwater flow model parameterization

The MODFLOW software suite is used to solve the groundwater flow equation under steady state conditions for unconfined aquifer using a three-dimensional finite difference approach (Harbaugh, 2005; Niswonger et al., 2011). The hydraulic head, h [L], is calculated as a function of the hydraulic conductivity, K [L T^{-1}], and the recharge rate, R [L T^{-1}], applied on top of the water column. At the surface of the model domain, the drain package (DRN) of MODFLOW (Harbaugh, 2005) accounts for the intersection of the groundwater table with the surface, and for the induced seepage. Overland flows and surface water reinfiltration are not integrated as remaining marginal in the conditions of temperate climate and low topographical gradients of the studied sites.

We use the FloPy Python package (Bakker et al., 2016) to set and handle simulations. To reduce uncertainties linked to potential flow across topographic boundaries, a buffer zone is added to the topographical catchment boundaries, increasing the modelled domain area by 10 %. The 3D model domain is discretized laterally using the regular mesh of the DEM, and vertically into 6 layers of equal thickness. Convergence tests have been performed to ensure the stability of the result independently of the numerical discretization. In agreement with field observations undertaken in the region, a homogeneous thickness of the aquifer, d [L], is set to a constant value of 30 m. This thickness represents the typical depth of the interface between the shallow

weathered/fractured zone with the underlying fresh bedrock (Dewandel et al., 2006; Roques et al., 2016; Mougin et al., 2008; Kolbe et al., 2016). The model assumes a uniform and isotropic hydraulic conductivity.

The recharge is estimated by the land EXternalized SURFace model SURFEX version 8.1 (Le Moigne et al., 2020). For more detailed information, the reader is referred to https://www.umr-cnrm.fr/surfex/. Supplied by meteorological variables, SURFEX computes the energy and water fluxes at the interfaces between soil, vegetation, and atmosphere (Noilhan and Mahfouf, 1996). The groundwater recharge of SURFEX is computed as the proportion of the water mobilized down to the aquifer after infiltrating through the soil column (Vergnes et al., 2020). SURFEX was supplied by the SAFRAN meteorological reanalysis (Vidal et al., 2010; Quintana-Seguí et al., 2008), available over the French metropolitan area at an 64 km^2 (8 x 8 km) resolution. Here, we took the steady-state recharge as the long-term average recharge rates computed over the period 1960-2019 and applied uniformly over the surface of the 3D domain.

2.3 Spatial distribution of observed stream network

The observed stream network is extracted from the French hydrographic network database BD TOPAGE as a vector format at the scale of 1:10 000 (IGN and OFB, 2019). The main vector file labelled "Cours d'eau" (Rivers) of the BD TOPAGE represents a majority of perennial sections of the stream network, i.e. filled and/or continuous-flow segments throughout the year. Note that the information classifying perennial or intermittent streams collected in the database is still under development to gain accuracy (Schneider et al., 2017). It has been rasterized at a grid resolution similar of the groundwater flow model in order to facilitate the comparison of the results (*WBT.VectorLinesToRaster*). Due to the uncertainty of the positioning of the stream network vector with respect to the DEM, an error of the order of a pixel is considered (plus or minus 75 m in this case). The influence of this error is analyzed in the results presented in section 3.1 (Figure 4). We also quantify the impacts of other DEM product resolutions by considering 5 other hydrographic network products from 3 different sources: the global-scale database HydroRIVERS (labelled case A), the French database BD TOPAGE (cases B, C and D), and local scale inventories (cases E and F) performed within the framework of the SAGE (Schéma d'Aménagement et de Gestion des Eaux The HydroRivers product is derived from the processing of the DEM at lower resolution (approximately 500 m at the equator), while the local inventories are completed by more detailed field observations. More information on these products can be found in Appendix A.

2.4 Calibration criteria between observed and simulated spatial patterns

For each pixel where seepage is simulated by the groundwater flow model, we trace the nearest downslope flowpath to the observed stream and compute its distance D_{so} [L] (*WBT.TraceDownslopeFlowpaths*) (Figure 2a). This function of WhiteToolBox uses the topographic structure to compute the path from cells on the surface to the catchment outlet. This procedure converts the initial discontinuous spatial pattern of seepage zones simulated by the groundwater flow model into a continuous stream network (Figure 2b).
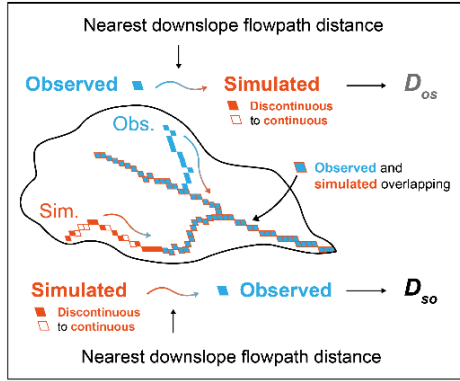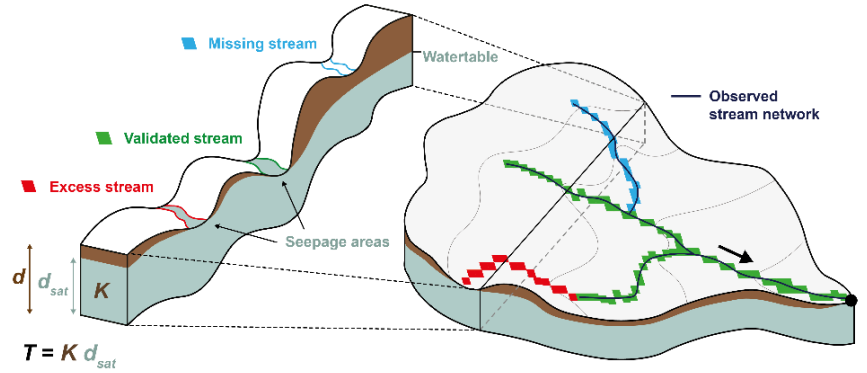
Figure 2. a) Definition of the main metrics used for calibration, with $\overline{D_{so}}$, the average distances computed from simulated stream
pixels (in orange) to the nearest (downslope flowpath) observed stream pixels (in blue), and $\overline{D_{os}}$ the average distances obtained
conversely. **b)** 3D conceptual diagram of the groundwater flow model and of a cross section through the catchment. Continuous
streams are generated from pixels where the simulated groundwater table intercepts the topography. By comparison with the
observed stream network, some of the simulated streams are correctly estimated (valid in green), over-estimated (excess in red), or
under-estimated (missing in blue).

The distances of the simulated stream network to the observed D_{so} are calculated and averaged into the criterion labelled $\overline{D_{so}}$.
(*WBT.DownslopeDistanceToStream*). High $\overline{D_{so}}$ values are characteristic of stream networks extending far away from the
observed steams. We also compute the mean distance of the observed to the simulated stream networks following a similar
procedure. The distance D_{os} [L] from each observed stream network pixel to the simulated stream is computed along the
steepest downslope path. In the following, we consider its average $\overline{D_{os}}$ obtained over all pixels of the observed streams. High
$\overline{D_{os}}$ values are characteristic of an usnderdeveloped stream network. The minimum absolute difference between $\overline{D_{so}}$ and $\overline{D_{os}}$
(Eq. (1)), labelled J, is used as the calibration criterion expressing the closest match of the observed and simulated streams or,
in other words, the most relevant combination of missing and excess streams (Figure 2):

$$J = |\overline{D_{so}} - \overline{D_{os}}|$$

(1)

$\overline{D_{so}}$ and $\overline{D_{os}}$ intersect when the calibration criterion J is met. This criterion based on both $\overline{D_{so}}$ and $\overline{D_{os}}$ achieves the best
equilibrium between over- and under-estimations.

At this point, we define the distance D_{optim} [L] as the average of $\overline{D_{so}}$ and $\overline{D_{os}}$ (Eq. (2)):

$$D_{optim} = \frac{\overline{D_{so}} + \overline{D_{os}}}{2}$$

(2)

The smaller the value of D_{optim}, the better is the match of the simulated seepage pattern and the observed stream network. D_{optim} will thus be used as an indicator of the calibration performance. In order to compare cases with different DEM resolution DEM_{res} [L], D_{optim} is normalized by the DEM resolution:

$$r_{optim} = \frac{D_{optim}}{DEM_{res}}$$

(3)

195   r_{optim} [-] should remain small to ensure the consistency of the observed and simulated stream networks. It will practically be limited to 2 considering that the mismatch cannot exceed the resolution of two pixels:

$$r_{optim} \leq 2$$

(4)

2.5   Estimating the optimal hydraulic conductivities

The model parameter K/R ratio is calibrated by minimizing the objective function defined by Eq. (1), for a given aquifer thickness (d). Optimization is performed by a dichotomy approach (Burden and Faires, 1985). The convergence criterion is

200   reached when K/R varies by less than 1 %. In order to ensure that K estimates are representative of catchment-scale processes driving the spatial distribution of the stream network, independently of the aquifer thickness set in the model, we computed the equivalent normalized transmissivity, T/R [-], by multiplying K/R by the average saturated aquifer thickness (d_{sat}) computed by the model at the catchment-scale (Figure 2b). In our modeling approach, K and d are input parameters of the model, while T is an output including the computed d_{sat}. Finally, optimal transmissivity T_{optim} and hydraulic conductivity

205   K_{optim} are evaluated assuming the applied average groundwater recharge rate, R, and under known aquifer thickness.

2.6   Testing the methodology on selected pilot catchments

The approach is deployed on 24 selected catchments located in Brittany and Normandy (France) (Figure 3), where an oceanic and temperate climate prevails. The average catchment area ranges from 12 to 141 km^2 with an average of 58 km^2 (Table 1),

210   which corresponds to an average of 61 800 elements for the domain model discretization. These catchments were selected because of the diversity of their geological and geomorphological settings. Most of them are also subject to extensive research activities for their importance in providing freshwater to the nearby cities (sites 1, 2, 3, 4, 5, 6, 15, 16, 18, 19) or flooding dynamics (sites 20, 21, 22, 23, 24). Some of these sites are also studied in collaboration with local stakeholders on issues related to water quality and river restoration (sites 8, 9, 10, 11, 12, 13 ,14, 17, 18 19) or within observatories and research

215   infrastructures (site 7: Long-Term Socio-Ecological Research (LTSER) "Zone Atelier Armorique (ZAAr)" and sites 17, 18, 19: French network of Critical Zone Observatories (OZCAR) "Ploemeur-Guidel CZO"). None of these catchments present any reservoir or stream obstacle that would significantly alter the stream network. The study sites cover 5 major lithologies

including: Brioverian schist (sedimentary rock), Paleozoic sandstone and schist (sedimentary rock), plutonic rocks (mainly granite), micaschist (metamorphic sedimentary rock) and limestone (sedimentary rock). Sites have a homogeneous lithology (1:1 000 000 scale) throughout the catchment except for 5 sites (sites 7, 8, 17, 18, 19) that present 2 lithologies.
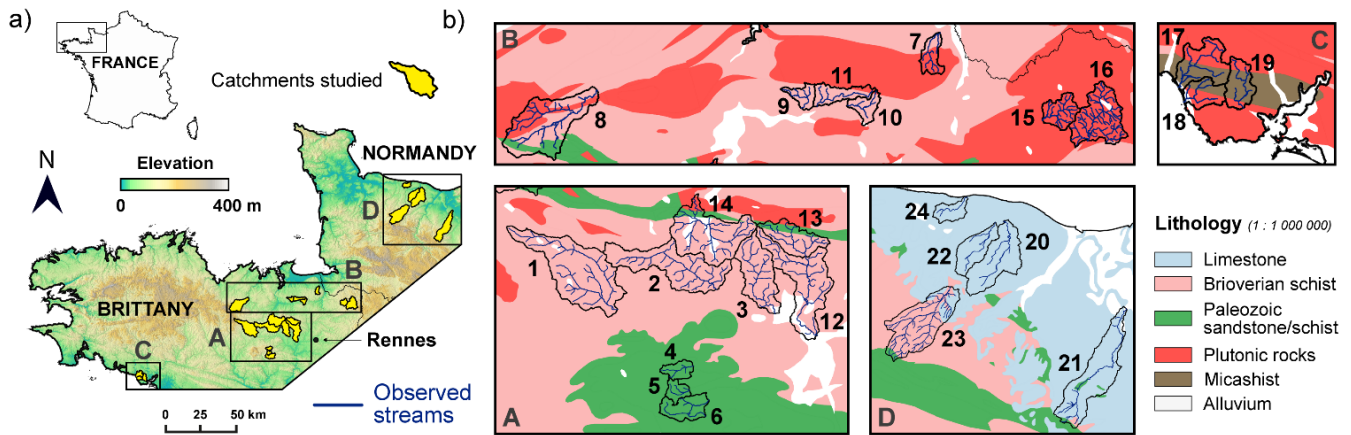
Figure 3. a) Location of the pilot catchments (Armorican Massif in Brittany and Normandy, North-Western part of France). b) Zoom on sites along with a simplified map of the main lithological units (1:1 000 000 scale) in sub-panels A, B, C and D.

3 Results

3.1 Detailed analysis of model results on a single site

Before presenting the results obtained for the ensemble of pilot sites, we first illustrate the results of the methodology on one specific site, the Canut catchment (Figure 3, site 6). We provide details on the different steps of the numerical method and assess their performance. The main results of the calibration method are presented in Figure 4. The dimensionless ratio K/R strongly controls the spatial distribution of the hydraulic head, i.e. the saturated aquifer thickness d_{sat}, the shape of the groundwater table, and its intersection with the surface (Figure 4a). As K/R increases, the head gradient decreases and progressively disconnects from the surface. This implies that the seepage areas become sparser, mostly organized downstream close to the catchment outlet. Inversely, lower values of K/R tend to expand the seepage patterns along the valleys and depressions towards the head of the catchment. Figure 4a shows the sensitivity of $\overline{D_{so}}$ and $\overline{D_{os}}$ considering 3 values of K/R. It confirms that the distance from the observed to the simulated stream network $\overline{D_{os}}$ increases with K/R and inversely that the distance from the simulated to the observed stream network $\overline{D_{so}}$ decreases with K/R.

High-order streams are accurately predicted in all three simulations as shown by the green pixels (Figure 4a). Low-order streams are more sensitive and drive most of the variations of $\overline{D_{so}}$ and $\overline{D_{os}}$ as shown by the evolving red to green pixels when changing K/R. In other words, the calibration is controlled by the spatial extent of the streams from the valleys to the headwaters

240 following the topographic depressions. D_{optim} is equal to 147 m and remains smaller than twice the resolution of the DEM indicating a close match of the observed streams (Figure 4b). Using the DEM resolution of 75 m as an indicator of uncertainty, K/R ranges between 1 458 and 7 082 (shaded area in Figure 4b), corresponding to an hydraulic conductivity ranging between 1.1 x 10^{-5} and 4.8 x 10^{-5} m s^{-1} for an estimated average recharge of 215 mm y^{-1}. In this case, the optimal hydraulic conductivity K_{optim} is estimated at 1.8 x 10^{-5} m s^{-1}. We deduce the optimal transmissivity T_{optim} of 5.1 x 10^{-4} m^2 s^{-1} considering an average

245 saturated thickness of 28.1 m simulated by the model (Figure 4b).
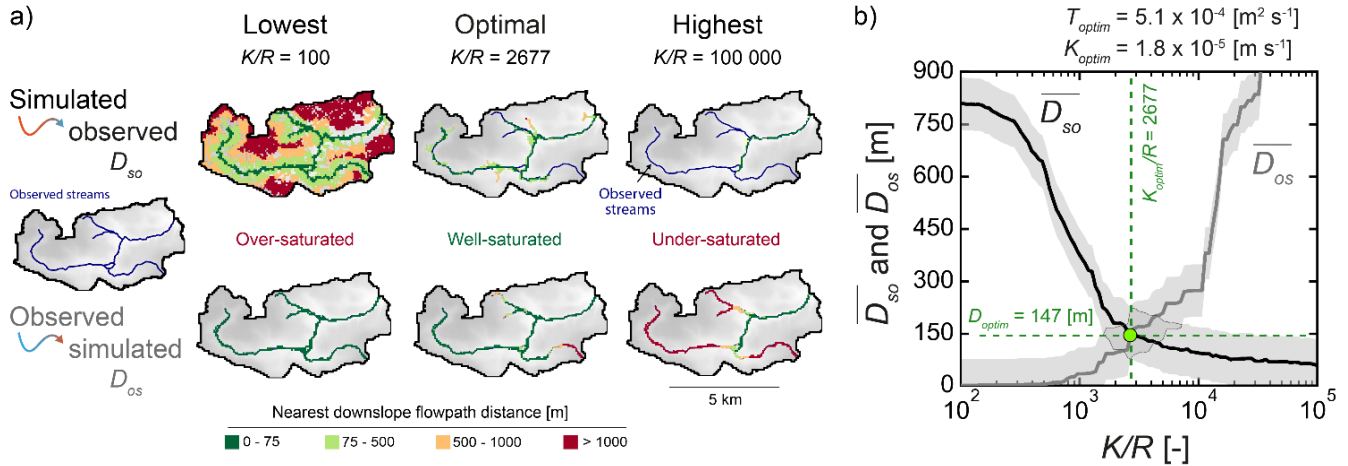
Figure 4. a) 2D map views of distances computed along the steepest slope from simulated stream pixels to the nearest observed ones (D_{so}) and from the observed stream pixels to the nearest simulated ones (D_{os}) for the Canut catchment. Results are presented for the lowest, optimal and highest K/R values explored. b) Average distances $\overline{D_{so}}$, and $\overline{D_{os}}$ as functions of K/R. The shaded areas in
250 grey around the curves correspond to the 75 m uncertainty range equal to the resolution the DEM. The optimal simulation is obtained for K_{optim}/R at the intersection between the two curves. At this point $\overline{D_{so}}$ and $\overline{D_{os}}$ are both equal to D_{optim} and, in this case, r_{optim} is close to 2. The optimal hydraulic conductivity estimated K_{optim} is derived by using the recharge rate provided by SURFEX, and T_{optim} is obtained considering the mean saturated aquifer thickness (d_{sat}). To further illustrate the methodology, an animated figure representing 2D map views of the simulated seepage areas as a function of K/R is available in the supplementary
255 material (Supplement 1) with the associated objective minimization function results in Appendix B.

We evaluate the impact of the maximum aquifer thickness on T_{optim} by running the calibration procedure considering five different values of d: 5, 10, 50, 100 and 300 m. We found that the simulated stream network matches the observed one for all thicknesses (d) (Figure 5a1, A to F). However, we found differences in the estimated T_{optim} (Figure 5a2). For cases C, D, E
260 and F, where the maximum aquifer thicknesses are greater than 30 m, the optimal transmissivity T_{optim} remains constant at around 4.0 x 10^{-4} m^2 s^{-1}. For cases A and B with smaller thicknesses (<30m), T_{optim} reach much larger values of 4.1 x 10^{-3} and 1.8 x 10^{-3} m^2 s^{-1} respectively. Such divergences come from the breakdown of the Dupuit-Forchheimer assumption. Small thicknesses bring the flow lines closer to the surface and widen the seepage areas (Bresciani et al., 2014), effects that must be offset by substantially higher hydraulic conductivities and transmissivities to lower the water table.

265   We also investigate the sensitivity of the resolutions of both the DEM (Figure 5b) and the observed stream network (Figure 5c) on the estimations of T_{optim}. The resolution of the DEM has only a minor influence on the estimation of optimal transmissivity, while the resolution of the stream network has a major impact. Figure 5b1 shows that the simulated stream network corresponds well to the observed network for the different DEM resolutions. However, the estimated optimal transmissivities vary significantly across the different cases (Figure 5b2). For cases C, D, and E, the estimated T_{optim} values

270   remain close to each other, ranging from 5.0 x 10^{-5} to 5.6 x 10^{-5} m^2 s^{-1}. For the case F, it reaches a value of 2.9 x 10^{-4} m^2 s^{-1} while for A and B it takes values of 1.9 x 10^{-3} and 9.7 x 10^{-4} m^2 s^{-1} respectively. For cases C to F, the r_{optim} criterion (Eq. (3)) remains close to 1 (from 0.5 to 1.8), smaller than the threshold of 2 (Eq. (4)). However, for the 5 and 25 m resolutions tested (cases A and B), the distances $\overline{D_{so}}$ and $\overline{D_{os}}$ are highly sensitive to the mismatch between an increasingly accurate DEM and a coarsely defined stream network. The main factor driving $\overline{D_{so}}$ and $\overline{D_{os}}$ is no longer the hydraulic conductivity but the mismatch

275   between the DEM and the observed stream network with r_{optim} values becoming larger (respectively 46.5 and 7.7 for the 5 and 25 m resolutions tested). These results emphasize that DEMs with too fine resolutions, here 5 and 25 m, cannot be used with the observed stream network selected in this study, at least at the current stage of the methodological development. Resolutions of 75 m and coarser lead however to consistent estimations of the hydraulic conductivity confirming the validity of the modeling approach.

280   We have systematically tested the method using six different stream network products issued by global, national, and local databases (Figure 5c1). These products display important differences in the extent and densities of the stream network coming from their origin and scale of observations (Appendix A). For case A, the global-scale product HydroRIVERS (Lehner et al., 2013) locates rivers away from the topographic valleys of the DEM, with consequently a D_{optim} value more than ten times larger than DEM_{res}. For cases B to F, the criterion r_{optim} (Eq. (3)) remains smaller than 2, the hydrographic network is well

285   captured and the method consistently estimate T_{optim} (Figure 5c2). T_{optim} varies over one order of magnitude from 2.0 x 10^{-4} to 3.8 x 10^{-3} m^2 s^{-1} and logically tends to decrease when the density and extent of the mapped stream network increases. Indeed, for a fixed recharge rate, lower transmissivities raise the groundwater table and broaden the headwater streams (Figure 5c, E and F). Conversely, higher values of T contract the hydrographic networks with streams located mainly at lower elevations (Figure 5c1, A and B). The extent of the stream system and the first-order stream locations appear to be highly sensitive to the

290   estimated transmissivity confirming its capacities to inform the hydraulic conductivity.
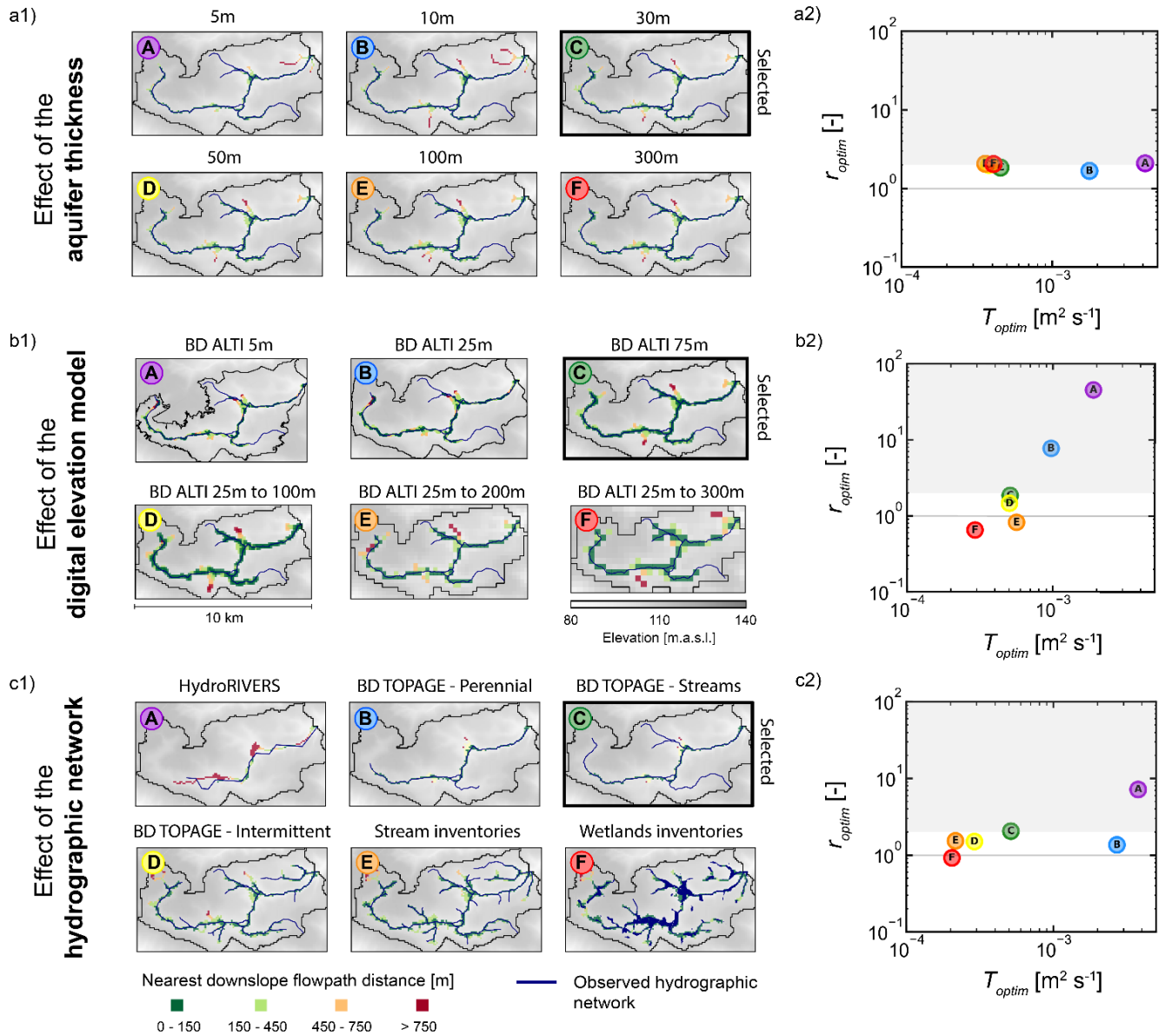
Figure 5. Sensitivity analysis of the method for the Canut catchment (site 6) to a) the DEM resolution, b) the density and extent of the steam network displayed by different stream network products, and c) the aquifer thickness. Left pictures (a1, b1, c1) show the downslope flowpath distances of the simulated stream pixels projected onto the observed reference stream network, for the $K_{optim}./R$. Right graphs (a2, b2, c2) show the r_{optim} as a function of T_{optim}.

3.2 Application to the ensemble of catchments

The method has been applied to the 23 other catchments (Figure 3) with the same DEM resolution of 75 m, product for the observed reference stream network, and aquifer thickness of 30 m. Both $\overline{D_{so}}$ and $\overline{D_{os}}$ were found to systematically intersect defining optimal D_{optim} (Figure 6) and K_{optim}/R values (Table 1). For 19 sites, the values of D_{optim} is less than 2 pixels (Figure 6), showing good consistency between the simulated and the observed stream network and K_{optim}/R vary between 1 397 to 19 687. Considering d_{sat} computed by the model, T_{optim} values range over one order of magnitude from 2.9×10^{-4} to 3.2×10^{-3} m^2 s^{-1} (Figure 6), resulting in K_{optim} values between 1.0×10^{-5} and 1.1×10^{-4} m s^{-1} (Table 1). The model captures correctly the features of the observed stream network even in the presence of singular topographical features such as extended depressions or sharp changes in slope (Gauvain et al., 2021; Schumm et al., 1995). This is especially the case on the site 7 where the seepage along the foot-slope issued by a steep slope transition (6 % on 1000 m of length) located along a lithological contact is well represented both by the model and in the observations as a significant and perennial groundwater spring/wetland (Vautier et al., 2019; Kolbe et al., 2016).
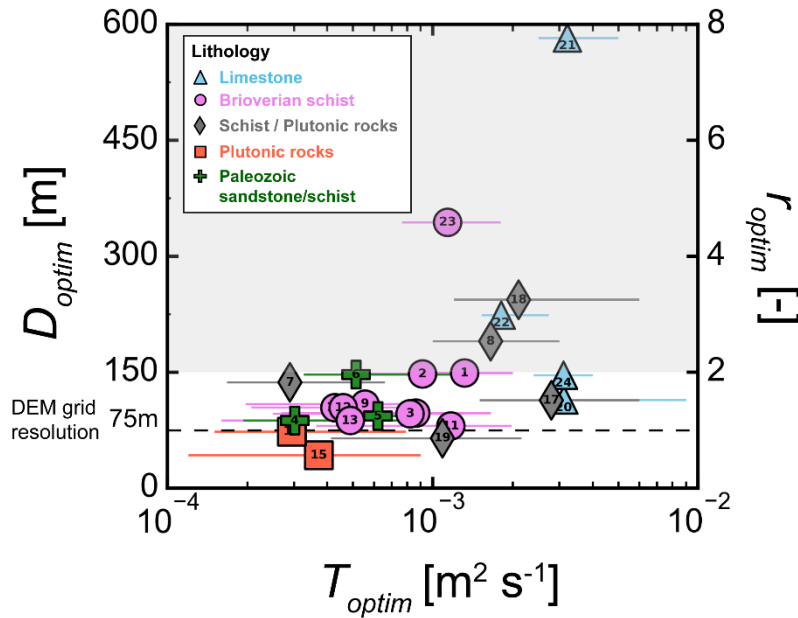
Figure 6. D_{optim} and r_{optim} criteria as functions of T_{optim} estimated for the 24 sites. The optimal transmissivity T_{optim} is obtained by considering K_{optim} and the mean saturated aquifer thickness d_{sat} computed. The shaded area corresponds to sites with $r_{optim} > 2$. The DEM resolution is 75 m and the aquifer thickness is 30 m. The error bars correspond to the estimated T_{optim} considering the DEM resolution as an uncertainty indicator.

Table 1. Main landscape characteristics, model input parameters, and modeling results, including hydraulic conductivities and transmissivities for the 24 catchments studied.

Catchment	Site ID	Main lithology	Area [km²]	Slope [%]	Drainage density [km⁻¹]	R [mm y⁻¹]	K_{optim}/R [-]	D_{optim} [m]	K_{optim} [m s⁻¹]	d_{sat} [m]	T_{optim} [m² s⁻¹]
Basance	15	Plutonic rocks	26	4.0	1.8	237	1783	40	1.3×10^{-5}	27.9	3.7×10^{-4}
Nancon	16		65	3.3	1.5	237	1397	73	1.1×10^{-5}	28.0	2.9×10^{-4}
Serein	4	Paleozoic sandstone/schist	13	3.7	0.8	226	1514	87	1.1×10^{-5}	27.7	3.0×10^{-4}
Cheze	5		12	2.5	0.8	226	3125	106	2.3×10^{-5}	27.5	6.2×10^{-4}
Canut	6		30	2.2	0.7	215	2677	147	1.8×10^{-5}	28.1	5.1×10^{-4}
Gael	1	Brioverian schist	132	2.5	0.7	201	7344	149	4.7×10^{-5}	28.0	1.3×10^{-3}
Garun	2		96	2.4	0.7	175	5938	144	3.3×10^{-5}	27.9	9.2×10^{-4}
Vaunoise	3		62	2.7	0.8	168	5469	106	2.9×10^{-5}	28.0	8.2×10^{-4}
Estret	9		14	2.0	1.0	161	3985	106	2.0×10^{-5}	27.6	5.6×10^{-4}
Linonlac	10		16	2.9	0.8	164	5860	97	3.1×10^{-5}	28.1	8.6×10^{-4}
Bouteille	11		24	2.9	0.8	161	8281	80	4.2×10^{-5}	28.0	1.2×10^{-3}
Flume	12		134	2.9	0.9	161	3243	105	1.6×10^{-5}	28.0	4.6×10^{-4}
Vignoc	13		41	3.0	0.9	172	3243	82	1.8×10^{-5}	27.8	4.9×10^{-4}
Neal	14		95	2.7	0.9	175	2774	107	1.5×10^{-5}	27.9	4.3×10^{-4}
Seulles	23		134	4.7	1.1	274	4688	342	4.0×10^{-5}	28.2	1.1×10^{-3}
Home	7	Schist/ Plutonic rocks	19	2.4	1.0	190	1739	135	1.0×10^{-5}	27.8	2.9×10^{-4}
Arguenon	8		103	4.7	0.8	234	7891	190	5.8×10^{-5}	28.2	1.7×10^{-3}
Guidel	17		24	3.8	1.0	307	10312	112	1.0×10^{-4}	28.1	2.8×10^{-3}
Lannenec	18		13	3.1	0.9	234	10078	243	7.5×10^{-5}	28.2	2.1×10^{-3}
Ploemeur	19		15	2.9	0.9	307	4063	81	3.9×10^{-5}	27.8	1.1×10^{-3}
Mue	20	Limestone	99	1.5	0.4	179	19687	114	1.1×10^{-4}	27.7	3.1×10^{-3}
Laizon	21		141	2.2	0.5	182	19375	581	1.1×10^{-4}	28.0	3.2×10^{-3}
Thue	22		52	1.9	0.5	172	12031	222	6.5×10^{-5}	27.8	1.8×10^{-3}
Gronde	24		25	1.7	0.4	179	19687	146	1.1×10^{-4}	27.6	3.1×10^{-3}

4   Discussion

4.1   A new calibration method for the assessment of effective catchment-scale hydraulic properties

We have presented a process-based groundwater modeling approach to assess effective catchment-scale hydraulic properties (K and T) from the sole information of the density and spatial extent of the stream network. The proposed method 1) simulates the stream network by physically representing the 3D groundwater flows, 2) quantifies the mismatch between observed and simulated stream networks through distance-based spatial indicators, and 3) calibrates the subsurface hydraulic properties by minimizing a performance criterion. We compare it with existing approaches and indicators.

Previous modeling approaches were mostly based on TOPMODEL applications (Blazkova et al., 2002; Güntner et al., 2004; Franks et al., 1998) or hillslope scale flows (Luo et al., 2010). They presented the advantage of simplicity but were limited in simple cases where flows are topography-driven. As the 1D hillslope-scale approach of Stoll and Weiler (2010), our 3D distributed- and process-based groundwater approach remains valid in conditions where the groundwater table is not a strict replicate of the topography becoming "recharge controlled" (Haitjema and Mitchell-Bruker, 2005). It also accounts for the discontinuities of the seepage structure coming from the irregular connections of the subsurface flows with the surface (Godsey and Kirchner, 2014; Whiting and Godsey, 2016; Warix et al., 2021). It follows numerous field observations and synthetic

experiments showing the strong influence of 3D groundwater flow organizations on the location of seepage zones (Goderniaux et al., 2013; Fleckenstein et al., 2006; Gauvain et al., 2021; Dohman et al., 2021).

Several indicators have been proposed to compare the spatial patterns of the modeled and observed saturated areas mostly based on cell-by-cell and cell-neighborhood approaches. This includes the likelihood measure (Franks et al., 1998; Blazkova et al., 2002), the Kappa goodness-of-fit statistic (Stoll and Weiler, 2010), the Euclidean distance between cells (Güntner et al., 2004). These indicators are essentially local and readily accessible from information on topography and stream networks. We propose more integrative indicators based on the distance between the observed and simulated stream networks computed along the steepest slope between them, as does the IDPR (Network Development and Persistence Index) to identify zones predominantly favorable to infiltration or runoff (Mardhel et al., 2021). The advantages of this procedure are to account for the topographical structure within the definition of the distances and to constrain the comparison on the best compromise between the over- and under-saturation, mainly driven by $\overline{D_{so}}$ and $\overline{D_{os}}$ respectively.

4.2 Comparison of estimated hydraulic conductivities with previously published values

As shown in Figure 6, the method predicts a distribution of T values that stands within one order of magnitude despite the broad range of lithological units investigated. Overall, our estimates of hydraulic properties are consistent with values found in previous studies conducted for similar sites and lithologic settings (Roques et al., 2016; Mougin et al., 2008; Dewandel et al., 2021; Cornette et al., 2022; Leray et al., 2012). We compared the estimated hydraulic conductivity, K_{optim}, with local to regional values found in the literature $K_{literature}$ (Figure 7). We focused on the comparison with local estimates from hydraulic tests or numerical groundwater models for 2 of the studied sites (Le Borgne et al., 2006; Kolbe et al., 2016; Jiménez-Martínez et al., 2013) or compiled in regional syntheses according to the lithology (Laurent et al., 2017; BRGM, 2018). Figure 7, shows a good agreement between our results and the other values. More specifically, the local values extracted for catchments 7 and 19 slightly underestimate the one from the literature by about 33 % (Figure 7, diamonds). The hydraulic conductivities derived from regional synthesis remain within the same order of magnitude with a limited overestimation of a factor of 2 (Figure 7, disks). This slight overestimation might result from testing methods as well as by the fact that local hydraulic tests are often carried out close to transmissive geological features of major interest for water supply. Our results were also compared to the ones compiled in the global scale database GLHYMPS (Huscroft et al., 2018). From the database, we derived equivalent hydraulic conductivities for each of the catchments. They range over 4 orders of magnitude, systematically lower by one to several orders of magnitude than our estimates (Appendix C). As shown in previous studies (de Graaf et al., 2020; Tashie et al., 2021), we find that the hydraulic conductivity dataset compiled in GLHYMPS may be locally underestimated.
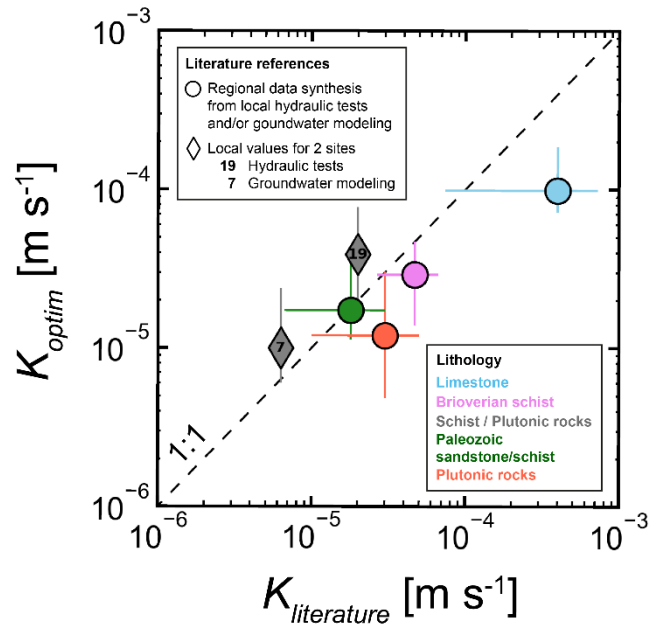
Figure 7. Comparison of K_{optim} obtained for the 24 catchments with values found in the literature $K_{literature}$ grouped into 2 categories according to the scale of investigation (local vs regional). Diamond: values from hydraulic tests and/or groundwater modeling compiled in regional syntheses according to lithologies (BRGM, 2018; Laurent et al., 2017). Disks: K obtained from local hydraulic tests for site 19 (Le Borgne et al., 2006; Jiménez-Martínez et al., 2013) and groundwater modelling for site 7 (Kolbe et al., 2016). The values provided in transmissivity by the literature are translated into hydraulic conductivities by using the same applied aquifer thickness of 30 m.

The results also show range of values consistent with those given by classical textbooks for the investigated lithologies (Freeze and Cherry, 1979; Domenico and Schwartz, 1990). Crystalline rocks characterized by weathering and fractures (Roques et al., 2014; Dewandel et al., 2006) have a lower hydraulic conductivity than sedimentary rocks, here represented by limestones with a karstic systems (IGN and OFB, 2019), displaying as expected higher conductivities. Lower conductivities suggest a high water table inducing a larger spatial extent of the stream network, confirmed by local knowledge, with a much higher observed drainage density for crystalline sites compared to limestone sites (Table 1). Although our results show evidence that effective conductivities are related to variations in dominant lithologies, it is also clear that other reported factors like erosion, bedrock weathering and fracturing may tend to homogenize the hydraulic properties under similar erosion/weathering settings (Luo et al., 2016; Yoshida and Troch, 2016; Jefferson et al., 2010; Litwin et al., 2022).

4.3 Sensitivity to input/model parameters and related improvements for broader applicability

380 The D_{optim} indicator (Eq. (2)) provides information on the level of uncertainty. It depends on the quality of the data (observed reference stream network and the DEM) and on the model assumptions. Five sites (8, 18, 21, 22 and 23) over the 23 sites studied display a low match of the simulated and observed stream networks ($r_{optim} > 2$) with D_{optim} values ranging from 190 to 581 m (Figure 6). Figure 8 maps the simulation results for these 5 sites. For site 18, the model predicts a seepage zone induced by a topographic depression representing potential ponds, lakes and wetlands, which are not in the observations. For

385 sites 21 and 22, the main differences are located at a non-reported subsurface flow in the observed stream network within a karstic system (IGN and OFB, 2019), however well represented by the model due to a topographic depression along this area. For site 23, the simulated flow at the bottom of the DEM valley appears to be parallel to the observed flow. In this case, it seems to be a registration error in the alignment of the stream location data within the DEM. For site 8, differences come principally from the model and, more specifically, from the assumption of a uniform hydraulic conductivity. For this site with

390 lateral lithologic heterogeneity, we found that the model underestimates the extent and density of the stream network in the part with dominant plutonic rocks, and overestimates them in the schists. On the site 8, the IDPR (Mardhel et al., 2021) indicates that the granitic area is less permeable than the schist area, and generally displays the limestone sites 21 and 22 primarily dominated by infiltration, consistent with our results.
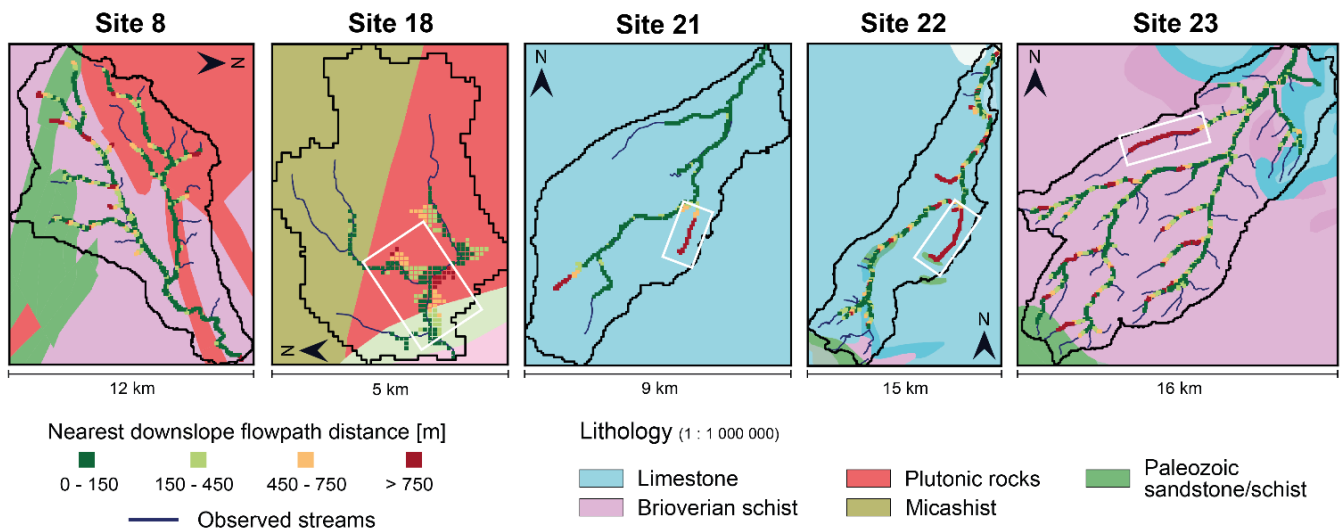
395 **Figure 8. For the 5 sites corresponding to $r_{optim} > 2$, representation of the observed stream network on top of the simplified geological map (1:1 000 000 scale), with the downslope flowpath distances of the simulated seepage areas projected to the observed streams. For site 8, differences are larger on the plutonic rocks. For the other sites, the white square identifies the area where differences are the largest.**

400   The high sensitivity of applied K/R with both the density and spatial extent of the observed stream network highlights the requirements to use high-quality stream products. Several issues may arise. First, river maps available in national to global databases are often incomplete compared to local databases compiled by stakeholders on direct field observations leading to an overestimation of the effective hydraulic properties. Second, artificial channels, drainage ditches and any other departure from the geomorphic equilibrium may alter the stream network system and lead to an overestimation of the hydraulic properties in highly impacted zones. Third, the resolution of the DEM and reference stream network must be close. Nevertheless, the

405 observed stream network layer could be adjusted to better match the DEM resolution.

    Major limitations and improvements may also arise from the assumptions of the hydrogeological model. The proposed methodology can be used with other parameterizations and model conceptualizations. The model domain can be extended, and the boundary conditions modified to better represent potentially longer and deeper regional groundwater circulations. If the

410 information is available, the method could be tested with heterogeneous recharge at the catchment scale. The geometry of the aquifer could be adapted, applying flat or irregular bottom aquifers based on geophysical measurements (Pasquet et al., 2022) or depth to bedrock databases (Shangguan et al., 2017; Hengl et al., 2017; Pelletier et al., 2016). Exponentially decreasing conductivity with depth can be applied to the model, in order to estimate the initial value of K at the surface or its characteristic decay depth. At the current stage of the method, catchment-scale lithological heterogeneities can be considered by applying

415 the methodology independently on sub-areas characterized by a homogeneous lithology. For example, on the studied site 8, application of the methodology on granite-dominated sub-catchments should result in lower K estimates than on the schist areas. Localized heterogeneities including weathering, fractures, faults, and other discontinuities cannot be identified. They should be explicitly introduced in the model and characterized by other methods.

420 **5   Conclusions**

    Global syntheses compiling accurate predictions of hydraulic properties of the subsurface are critically needed to predict water resources availabilities (Fan et al., 2019) in ungauged catchments (Sivapalan et al., 2003; Hrachowitz et al., 2013) and to assess the impact of hillslope- and catchment-scale hydrology on global change predictions (Taylor et al., 2013). Besides the climatic forcing data, requiring only a stream network map to calibrate a groundwater flow model built from a DEM, the approach

425 presented in this article addresses this challenge, specifically for ungauged basins. Under the assumption that the transmissivity (hydraulic conductivity integrated over the saturated aquifer thickness) controls the extension and density of the hydrographic network, the approach calibrates the effective hydraulic properties on the stream network. The resolution of the stream network and DEM should be consistent. We showed that the spatialized performance criterion based on the distances between the simulated and observed stream network achieves an equilibrium between over- and under-saturation of the underlying

430 groundwater system, as well as an equilibrium between over- and underestimation of the stream network extent. The resulting estimated K values are consistent with local values found in the literature.

A major advantage is the ease of deployment and transferability of the methodology to other catchments. Although the proposed methodology is limited to unconfined aquifers and particularly suited to contexts with significant subsurface-surface interactions, where groundwater primarily feeds streams, it aims to be deployed at multiple spatial scales by taking advantage

435 of databases compiling topographic, hydrologic, and climate information. Such deployment improving subsurface characterization from surface information would leverage the current development in crowdsourcing (Etter et al., 2020) and innovations in remote sensing (Biancamaria et al., 2016) that now provide high resolution surface DEM products (Hawker et al., 2022; Yamazaki et al., 2017), and mapping of hydrographic networks (Grill et al., 2019; Yamazaki et al., 2019) distinguishing the perennial and intermittent streams (Fovet et al., 2021; Messager et al., 2021).

440

Appendices

Appendix A: Hydrographic network products information.

445 **Global database:** HydroRIVERS (available on this website: https://www.hydrosheds.org/page/hydrorivers) (Linke et al., 2019) is derived from HydroSHEDS (Lehner et al., 2013), a mapping product that provides stream information for regional and global-scale applications, based on a grid resolution of 15 arc-seconds (approximately 500 m at the equator).

National database: The BD TOPAGE (available on this website: https://bdtopage.eaufrance.fr) database classifies streams as perennial or intermittent based on historical photogrammetric reconstructions.

450 **Local database:** The local stream and wetland inventory maps are based on observations and field surveys validated by the "Schéma d'Aménagement et de Gestion des Eaux (SAGE) (available on this website: https://sdage-sage.eau-loire-bretagne.fr/home.html).

Appendix B: Objective function of the calibration criteria.
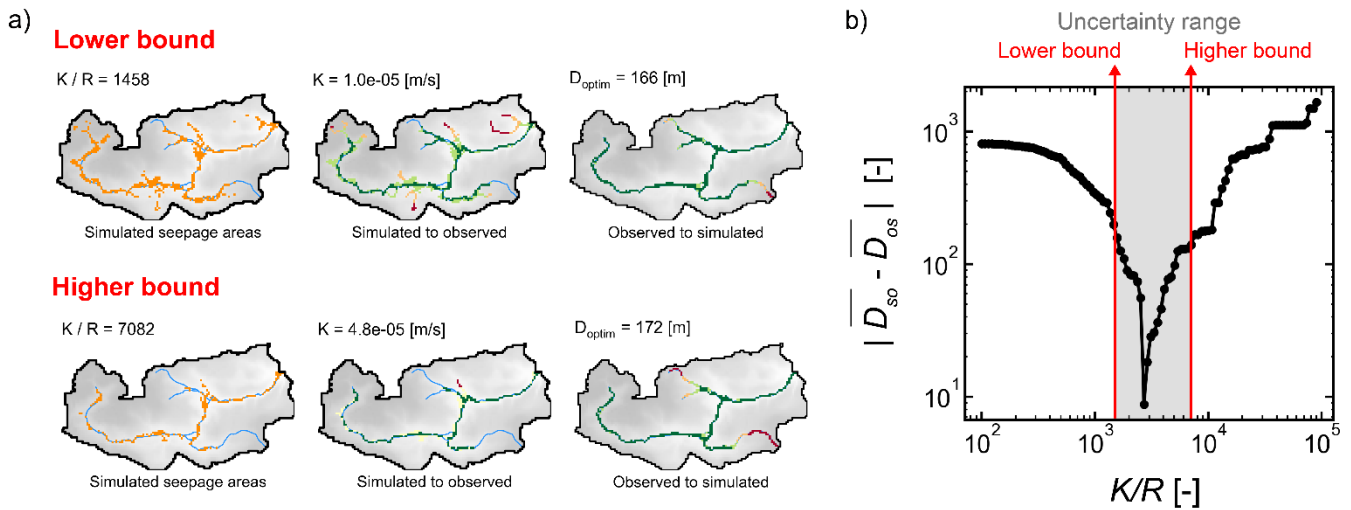
455 **Fig. B1. For the Canut catchment (site 6), a) 2D map views of simulated seepage areas and nearest downslope flowpath distances (simulated to observed and observed to simulated) for the two K/R at the bounds of the uncertainty (lower and higher), and b) the objective function based on the developed performance criteria obtained.**

Appendix C: Comparison with the GLobal HYdrogeology MaPS (GLHYMPS 2.0) permeability.
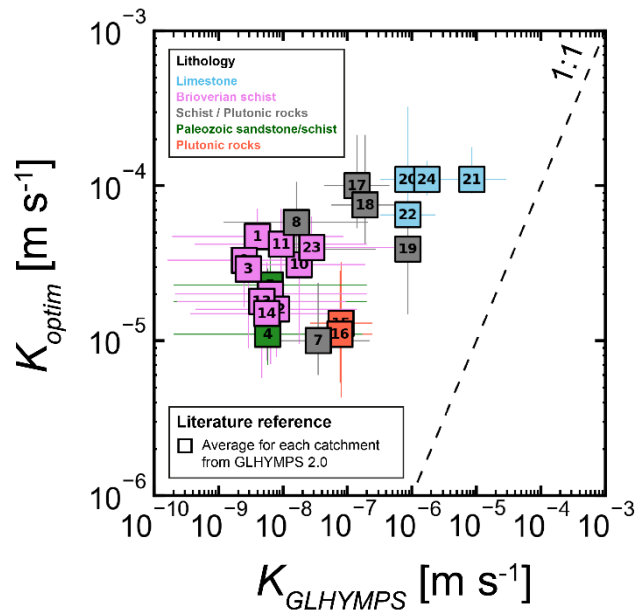
Fig. C1. Comparison of K_{optim} obtained for the 24 catchments with values of the literature provided by the GLHYMPS 2.0 global permeability map (Huscroft et al., 2018), $K_{GLHYMPS}$, averaged over each catchment.

Supplements

Supplement 1: Evolution of the simulated stream network as a function of K/R.

The animated figure in a *.gif format is provided in a *.zip archive.

Fig. S1. Animated figure at the scale of the Canut catchment (site 6) representing the 2D map views of simulated seepage areas and nearest downslope flowpath distances (simulated to observed and observed to simulated). The maps come from an exploration of a wide range K/R [100 to 90 000].

Code and data availability

A Python code to test the method is available online on a shared repository:

https://github.com/RonanAbherve/stream-network_beta

Author contribution

All co-authors were involved in the conceptualization of the original methods, identification of the research questions and the interpretation of the results. Ronan Abhervé (RA) and Alexandre Gauvain developed the model, performed the simulations, and analyzed the results. RA created the figures and prepared the first draft of the manuscript. All co-authors reviewed and edited the manuscript.

Competing interests

The authors declare that they do not have any conflict of interest.

Acknowledgments

This work was funded by Eau du Bassin Rennais and Rennes Métropole, through the "Eaux et Territoires" ("Water and Territories") research chairs of the Foundation of the University of Rennes. Clément Roques acknowledges financial supports from the Rennes Métropole research chair "Ressource en Eau du Futur" and the European project WATERLINE, project id CHIST-ERA-19-CES-006. Alexandre Gauvain acknowledges funding from the RIVAGES Normands 2100 project. The investigations also benefited from the support of the Network of hydrogeological research sites (H+) Observatory and the Research Observatory French network of Critical Zone Observatories: Research and Applications (OZCAR-RI).

References

Achtziger-Zupančič, P., Loew, S., and Mariéthoz, G.: A new global database to improve predictions of permeability distribution in crystalline rocks at site scale, J. Geophys. Res. Solid Earth, 122, 3513–3539, https://doi.org/10.1002/2017JB014106, 2017.

Alley, W. M., Healy, R. W., LaBaugh, J. W., and Reilly, T. E.: Flow and storage in groundwater systems, Science (80-.)., 296, 1985–1990, https://doi.org/10.1126/science.1067123, 2002.

Anderson, M. P., Woessner, W. W., and Hunt, R. J.: Applied groundwater modeling : simulation of flow and advective transport, Second Edi., Elsevier, AP Academic press is an imprint of Elsevier, Amsterdam, ixi, 564 pp., 2015.

Bakker, M., Post, V., Langevin, C. D., Hughes, J. D., White, J. T., Starn, J. J., and Fienen, M. N.: Scripting MODFLOW Model Development Using Python and FloPy, 54, 733–739, https://doi.org/10.1111/gwat.12413, 2016.

Barclay, J. R., Starn, J. J., Briggs, M. A., and Helton, A. M.: Improved Prediction of Management-Relevant Groundwater Discharge Characteristics Throughout River Networks, Water Resour. Res., 56, 1–19, https://doi.org/10.1029/2020WR028027, 2020.

Beven, K., Asadullah, A., Bates, P., Blyth, E., Chappell, N., Child, S., Cloke, H., Dadson, S., Everard, N., Fowler, H. J., Freer, J., Hannah, D. M., Heppell, K., Holden, J., Lamb, R., Lewis, H., Morgan, G., Parry, L., and Wagener, T.: Developing observational methods to drive future hydrological science: Can we make a start as a community?, Hydrol. Process., 34, 868–873, https://doi.org/10.1002/hyp.13622, 2020.

Beven, K. J. and Kirkby, M. J.: A physically based, variable contributing area model of basin hydrology, Hydrol. Sci. Bull., 24, 43–69, https://doi.org/10.1080/02626667909491834, 1979.

Biancamaria, S., Lettenmaier, D. P., and Pavelsky, T. M.: The SWOT Mission and Its Capabilities for Land Hydrology, Surv. Geophys., 37, 307–337, https://doi.org/10.1007/s10712-015-9346-y, 2016.

Blazkova, S., Beven, K. J., and Kulasova, A.: On constraining TOPMODEL hydrograph simulations using partial saturated area information, Hydrol. Process., 16, 441–458, https://doi.org/10.1002/hyp.331, 2002.

Blöschl, G., Bierkens, M. F. P., Chambel, A., Cudennec, C., Destouni, G., Fiori, A., Kirchner, J. W., McDonnell, J. J., Savenije, H. H. G., Sivapalan, M., Stumpp, C., Toth, E., Volpi, E., Carr, G., Lupton, C., Salinas, J., Széles, B., Viglione, A., Aksoy, H., Allen, S. T., Amin, A., Andréassian, V., Arheimer, B., Aryal, S. K., Baker, V., Bardsley, E., Barendrecht, M. H., Bartosova, A., Batelaan, O., Berghuijs, W. R., Beven, K., Blume, T., Bogaard, T., Borges de Amorim, P., Böttcher, M. E., Boulet, G., Breinl, K., Brilly, M., Brocca, L., Buytaert, W., Castellarin, A., Castelletti, A., Chen, X., Chen, Y., Chen, Y., Chifflard, P., Claps, P., Clark, M. P., Collins, A. L., Croke, B., Dathe, A., David, P. C., de Barros, F. P. J., de Rooij, G., Di Baldassarre, G., Driscoll, J. M., Duethmann, D., Dwivedi, R., Eris, E., Farmer, W. H., Feiccabrino, J., Ferguson, G., Ferrari, E., Ferraris, S., Fersch, B., Finger, D., Foglia, L., Fowler, K., Gartsman, B., Gascoin, S., Gaume, E., Gelfan, A., Geris, J., Gharari, S., Gleeson, T., Glendell, M., Gonzalez Bevacqua, A., González-Dugo, M. P., Grimaldi, S., Gupta, A. B., Guse, B., Han, D., Hannah, D., Harpold, A., Haun, S., Heal, K., Helfricht, K., Herrnegger, M., Hipsey, M., Hlaváčiková, H., Hohmann, C., Holko, L., Hopkinson, C., Hrachowitz, M., Illangasekare, T. H., Inam, A., Innocente, C., Istanbulluoglu, E., Jarihani, B., et al.: Twenty-three unsolved problems in hydrology (UPH) – a community perspective, Hydrol. Sci. J., 64, 1141–1158, https://doi.org/10.1080/02626667.2019.1620507, 2019.

Le Borgne, T., Bour, O., Paillet, F. L., and Caudal, J. P.: Assessment of preferential flow path connectivity and hydraulic properties at single-borehole and cross-borehole scales in a fractured aquifer, J. Hydrol., 328, 347–359, https://doi.org/10.1016/j.jhydrol.2005.12.029, 2006.

Bravo, H. R., Jiang, F., and Hunt, R. J.: Using groundwater temperature data to constrain parameter estimation in a groundwater flow model of a wetland system, Water Resour. Res., 38, 28-1-28–14, https://doi.org/10.1029/2000wr000172, 2002.

Bresciani, E., Davy, P., and De Dreuzy, J. R.: Is the Dupuit assumption suitable for predicting the groundwater seepage area in hillslopes?, Water Resour. Res., 50, 2394–2406, https://doi.org/10.1002/2013WR014284, 2014.

BRGM: Tectonic-lithostratigraphic log with evolution of hydrodynamic parameters according to lithological sets, SIGES Bretagne - Système d'information pour la Gest. des eaux Souterr. en Bretagne, 2018.

Brutsaert, W. and Nieber, J. L.: Regionalized Drought Flow Hydrographs From a Mature Glaciated Plateau, Water Resour. Res., 13, 1977.

Burden, R. L. and Faires, J. D.: "2.1 The Bisection Algorithm", Numerical Analysis (3rd ed.), PWS Publishers, 1985.

Carrera, J., Alcolea, A., Medina, A., Hidalgo, J., and Slooten, L. J.: Inverse problem in hydrogeology, Hydrogeol. J., 13, 206–222, https://doi.org/10.1007/s10040-004-0404-7, 2005.

Chow, R., Frind, M. E., Frind, E. O., Jones, J. P., Sousa, M. R., Rudolph, D. L., Molson, J. W., and Nowak, W.: Delineating baseflow contribution areas for streams – A model and methods comparison, J. Contam. Hydrol., 195, 11–22, https://doi.org/10.1016/j.jconhyd.2016.11.001, 2016.

Comunian, A. and Renard, P.: Introducing wwhypda: A world-wide collaborative hydrogeological parameters database, Hydrogeol. J., 17, 481–489, https://doi.org/10.1007/s10040-008-0387-x, 2009.

Cornette, N., Roques, C., Boisson, A., Courtois, Q., Marçais, J., Launay, J., Pajot, G., Habets, F., and de Dreuzy, J.-R.: Hillslope-scale exploration of the relative contribution of base flow, seepage flow and overland flow to streamflow dynamics, J. Hydrol., https://doi.org/Submitted, 2022.

Cromwell, E., Shuai, P., Jiang, P., Coon, E. T., Painter, S. L., Moulton, J. D., Lin, Y., and Chen, X.: Estimating Watershed Subsurface Permeability From Stream Discharge Data Using Deep Neural Networks, Front. Earth Sci., 9, 1–13, https://doi.org/10.3389/feart.2021.613011, 2021.

Cuthbert, M. O., Gleeson, T., Moosdorf, N., Befus, K. M., Schneider, A., Hartmann, J., and Lehner, B.: Global patterns and dynamics of climate–groundwater interactions, Nat. Clim. Chang., 9, 137–141, https://doi.org/10.1038/s41558-018-0386-4, 2019.

Day, D. G.: Lithologic controls of drainage density : a stud of six small rural catchments in New England , N . S . W ., 7, 339–351, 1980.

de Graaf, I., Condon, L., and Maxwell, R.: Hyper-Resolution Continental-Scale 3-D Aquifer Parameterization for Groundwater Modeling, Water Resour. Res., 56, 1–14, https://doi.org/10.1029/2019WR026004, 2020.

Dembélé, M., Hrachowitz, M., Savenije, H. H. G., Mariéthoz, G., and Schaefli, B.: Improving the Predictive Skill of a Distributed Hydrological Model by Calibration on Spatial Patterns With Multiple Satellite Data Sets, Water Resour. Res., 56, 1–26, https://doi.org/10.1029/2019WR026085, 2020.

Devauchelle, O., Petroff, A. P., Seybold, H. F., and Rothman, D. H.: Ramification of stream networks, Proc. Natl. Acad. Sci. U. S. A., 109, 20832–20836, https://doi.org/10.1073/pnas.1215218109, 2012.

Dewandel, B., Lachassagne, P., Wyns, R., Maréchal, J. C., and Krishnamurthy, N. S.: A generalized 3-D geological and hydrogeological conceptual model of granite aquifers controlled by single or multiphase weathering, J. Hydrol., 330, 260–284, https://doi.org/10.1016/j.jhydrol.2006.03.026, 2006.

Dewandel, B., Boisson, A., Amraoui, N., Caballero, Y., Mougin, B., Baltassat, J. M., and Maréchal, J. C.: Improving our ability to model crystalline aquifers using field data combined with a regionalized approach for estimating the hydraulic conductivity field, J. Hydrol., 601, https://doi.org/10.1016/j.jhydrol.2021.126652, 2021.

Dietrich, W. E. and Dunne, T.: The channel head, Channel Netw. Hydrol., eds Beven, 175–219, 1993.

Dohman, J. M., Godsey, S. E., and Hale, R. L.: Three-Dimensional Subsurface Flow Path Controls on Flow Permanence, Water Resour. Res., 57, 1–18, https://doi.org/10.1029/2020WR028270, 2021.

Domenico, P. A. and Schwartz, F. W.: Physical and chemical Hydrogeology, John Wiley & Sons, Inc., 1990.

Dunne, T.: Formation and controls of channel networks, 1975.

Eckhardt, K. and Ulbrich, U.: Potential impacts of climate change on groundwater recharge and streamflow in a central European low mountain range, J. Hydrol., 284, 244–252, https://doi.org/10.1016/j.jhydrol.2003.08.005, 2003.

Elshall, A. S., Arik, A. D., El-Kadi, A. I., Pierce, S., Ye, M., Burnett, K. M., Wada, C. A., Bremer, L. L., and Chun, G.: Groundwater sustainability: a review of the interactions between science and policy, Environ. Res. Lett., 15, https://doi.org/10.1088/1748-9326/ab8e8c, 2020.

Etter, S., Strobl, B., Seibert, J., and van Meerveld, H. J. I.: Value of Crowd-Based Water Level Class Observations for Hydrological Model Calibration, Water Resour. Res., 56, 1–17, https://doi.org/10.1029/2019WR026108, 2020.

Fan, Y.: Groundwater in the Earth's critical zone: Relevance to large-scale patterns and processes, Water Resour. Res., 51, 3052–3069, https://doi.org/10.1002/2015WR017037, 2015.

Fan, Y., Li, H., and Miguez-Macho, G.: Global Patterns of Groundwater Table Depth, Science (80-.)., 339, 940–943, https://doi.org/10.1126/science.1229881, 2013.

Fan, Y., Richard, S., Bristol, R. S., Peters, S. E., Ingebritsen, S. E., Moosdorf, N., Packman, A., Gleeson, T., Zaslavsky, I., Peckham, S., Murdoch, L., Fienen, M., Cardiff, M., Tarboton, D., Jones, N., Hooper, R., Arrigo, J., Gochis, D., Olson, J., and Wolock, D.: DigitalCrust - a 4D data system of material properties for transforming research on crustal fluid flow, 15, 372–379, https://doi.org/10.1111/gfl.12114, 2015.

Fan, Y., Clark, M., Lawrence, D. M., Swenson, S., Band, L. E., Brantley, S. L., Brooks, P. D., Dietrich, W. E., Flores, A., Grant, G., Kirchner, J. W., Mackay, D. S., McDonnell, J. J., Milly, P. C. D., Sullivan, P. L., Tague, C., Ajami, H., Chaney, N., Hartmann, A., Hazenberg, P., McNamara, J., Pelletier, J., Perket, J., Rouholahnejad-Freund, E., Wagener, T., Zeng, X., Beighley, E., Buzan, J., Huang, M., Livneh, B., Mohanty, B. P., Nijssen, B., Safeeq, M., Shen, C., van Verseveld, W., Volk, J., and Yamazaki, D.: Hillslope Hydrology in Global Change Research and Earth System Modeling, Water Resour. Res., 1737–1772, https://doi.org/10.1029/2018WR023903, 2019.

Fleckenstein, J. H., Niswonger, R. G., and Fogg, G. E.: River-aquifer interactions, geologic heterogeneity, and low-flow management, Ground Water, 44, 837–852, https://doi.org/10.1111/j.1745-6584.2006.00190.x, 2006.

Fovet, O., Belemtougri, A., Boithias, L., Marylise, J. C., Kevin, C., and Braud, I.: Intermittent rivers and ephemeral streams : Perspectives for critical zone science and research on socio-ecosystems, 1–33, https://doi.org/10.1002/wat2.1523, 2021.

Franks, S. W., Gineste, P., Beven, K. J., and Merot, P.: On constraining the predictions of a distributed model: The incorporation of fuzzy estimates of saturated areas into the calibration process, Water Resour. Res., 34, 787–797, https://doi.org/10.1029/97WR03041, 1998.

Freeze, R. A. and Cherry, J. A.: Groundwater, edited by: Prentice-Hall, Englewood Cliffs, N.J., 604 pp., 1979.

Gauvain, A., Leray, S., Marçais, J., and Roques, C.: Geomorphological Controls on Groundwater Transit Times : A Synthetic Analysis at the Hillslope Scale Water Resources Research, i, 1–22, https://doi.org/10.1029/2020WR029463, 2021.

Gleeson, T. and Manning, A. H.: Regional groundwater flow in mountainous terrain: Three-dimensional simulations of topographic and hydrogeologic controls, Water Resour. Res., 44, https://doi.org/10.1029/2008WR006848, 2008.

590 Gleeson, T., Moosdorf, N., Hartmann, J., and van Beek, L. P. H.: A glimpse beneath earth's surface: GLobal HYdrogeology MaPS (GLHYMPS) of permeability and porosity, Geophys. Res. Lett., 41, 3891–3898, https://doi.org/10.1002/ 2014GL059856, 2014.

Gleeson, T., Wagener, T., Döll, P., Zipper, S. C., West, C., Wada, Y., Taylor, R., Scanlon, B., Rosolem, R., Rahman, S., Oshinlaja, N., Maxwell, R., Lo, M. H., Kim, H., Hill, M., Hartmann, A., Fogg, G., Famiglietti, J. S., Ducharne, A., De Graaf, I., Cuthbert, M., Condon, L., Bresciani, E., and Bierkens, M. F. P.: GMD perspective: The quest to improve the evaluation of groundwater representation in continental-to global-scale models, Geosci. Model Dev., 14, 7545–7571, https://doi.org/10.5194/gmd-14-7545-2021, 2021.

595 Goderniaux, P., Davy, P., Bresciani, E., de Dreuzy, J. R., and Le Borgne, T.: Partitioning a regional groundwater flow system into shallow local and deep regional flow compartments, Water Resour. Res., 49, 2274–2286, https://doi.org/10.1002/wrcr.20186, 2013.

Godsey, S. E. and Kirchner, J. W.: Dynamic, discontinuous stream networks: Hydrologically driven variations in active drainage density, flowing channels and stream order, Hydrol. Process., 28, 5791–5803, https://doi.org/10.1002/hyp.10310, 2014.

Grayson, R. B. and Blöschl, G.: Spatial Patterns in Catchment Hydrology: Observations and Modelling, Cambridge, UK, 404 pp., 2000.

600 Grill, G., Lehner, B., Thieme, M., Geenen, B., Tickner, D., Antonelli, F., Babu, S., Borrelli, P., Cheng, L., Crochetiere, H., Ehalt Macedo, H., Filgueiras, R., Goichot, M., Higgins, J., Hogan, Z., Lip, B., McClain, M. E., Meng, J., Mulligan, M., Nilsson, C., Olden, J. D., Opperman, J. J., Petry, P., Reidy Liermann, C., Sáenz, L., Salinas-Rodríguez, S., Schelle, P., Schmitt, R. J. P., Snider, J., Tan, F., Tockner, K., Valdujo, P. H., van Soesbergen, A., and Zarfl, C.: Mapping the world's free-flowing rivers, Nature, 569, 215–221, https://doi.org/10.1038/s41586-019-1111-9, 2019.

Güntner, A., Seibert, J., and Uhlenbrook, S.: Modeling spatial patterns of saturated areas: An evaluation of different terrain indices, Water Resour. Res., 40, 605 1–19, https://doi.org/10.1029/2003WR002864, 2004.

Haitjema, H. M. and Mitchell-Bruker, S.: Are water tables a subdued replica of the topography?, Ground Water, 43, 781–786, https://doi.org/10.1111/j.1745-6584.2005.00090.x, 2005.

Harbaugh, A. W.: MODFLOW-2005 : the U.S. Geological Survey modular ground-water model--the ground-water flow process, Techniques and Methods, https://doi.org/10.3133/tm6A16, 2005.

610 Hartmann, J. and Moosdorf, N.: The new global lithological map database GLiM: A representation of rock properties at the Earth surface, Geochemistry, Geophys. Geosystems, 13, 1–37, https://doi.org/10.1029/2012GC004370, 2012.

Hawker, L., Uhe, P., Paulo, L., Sosa, J., Savage, J., Sampson, C., and Neal, J.: A 30 m global map of elevation with forests and buildings removed, Environ. Res. Lett., 17, 024016, https://doi.org/10.1088/1748-9326/ac4d4f, 2022.

Hengl, T., De Jesus, J. M., Heuvelink, G. B. M., Gonzalez, M. R., Kilibarda, M., Blagotić, A., Shangguan, W., Wright, M. N., Geng, X., Bauer-Marschallinger, 615 B., Guevara, M. A., Vargas, R., MacMillan, R. A., Batjes, N. H., Leenaars, J. G. B., Ribeiro, E., Wheeler, I., Mantel, S., and Kempen, B.: SoilGrids250m: Global gridded soil information based on machine learning, 1–40 pp., https://doi.org/10.1371/journal.pone.0169748, 2017.

Holman, I. P., Allen, D. M., Cuthbert, M. O., and Goderniaux, P.: Towards best practice for assessing the impacts of climate change on groundwater, Hydrogeol. J., 20, 1–4, https://doi.org/10.1007/s10040-011-0805-3, 2012.

Hrachowitz, M., Savenije, H. H. G., Blöschl, G., McDonnell, J. J., Sivapalan, M., Pomeroy, J. W., Arheimer, B., Blume, T., Clark, M. P., Ehret, U., Fenicia, 620 F., Freer, J. E., Gelfan, A., Gupta, H. V., Hughes, D. A., Hut, R. W., Montanari, A., Pande, S., Tetzlaff, D., Troch, P. A., Uhlenbrook, S., Wagener, T., Winsemius, H. C., Woods, R. A., Zehe, E., and Cudennec, C.: A decade of Predictions in Ungauged Basins (PUB)-a review, Hydrol. Sci. J., 58, 1198–1255, https://doi.org/10.1080/02626667.2013.803183, 2013.

Hsieh, P. A., Bredehoeft, J. D., and Farr, J. M.: Determination of aquifer transmissivity from Earth tide analysis, Water Resour. Res., 23, 1824–1832, https://doi.org/10.1029/WR023i010p01824, 1987.

625 Huscroft, J., Gleeson, T., Hartmann, J., and Börker, J.: Compiling and Mapping Global Permeability of the Unconsolidated and Consolidated Earth: GLobal HYdrogeology MaPS 2.0 (GLHYMPS 2.0), Geophys. Res. Lett., 45, 1897–1904, https://doi.org/10.1002/2017GL075860, 2018.

IGN: Le modèle numérique de terrain (MNT) maillé qui décrit le relief du territoire français à moyenne échelle BD ALTI® version 2021, Information Géographique sur l'Eau et Institut National de l'Information Géographique et Forestière, 2021.

IGN and OFB: Jeu de données des cours d'eau de France métropolitaine BD TOPAGE® version 2019, Office Français de la Biodiversité (OFB) - Information 630 Géographique sur l'Eau et Institut National de l'Information Géographique et Forestière, 2019.

Jefferson, A., Grant, G. E., Lewis, S. L., and Lancaster, S. T.: Coevolution of hydrology and topography on a basalt landscape in the Oregon Cascade Range, USA, Earth Surf. Process. Landforms, 35, 803–816, https://doi.org/10.1002/esp.1976, 2010.

Jiménez-Martínez, J., Longuevergne, L., Le Borgne, T., Davy, P., Russian, A., and Bour, O.: Temporal and spatial scaling of hydraulic response to recharge in fractured aquifers: Insights from a frequency domain analysis, Water Resour. Res., 49, 3007–3023, https://doi.org/10.1002/wrcr.20260, 2013.

635 Kolbe, T., Marçais, J., Thomas, Z., Abbott, B. W., de Dreuzy, J.-R., Rousseau-Gueutin, P., Aquilina, L., Labasque, T., and Pinay, G.: Coupling 3D groundwater

modeling with CFC-based age dating to classify local groundwater circulation in an unconfined crystalline aquifer, J. Hydrol., 543, 31–46, https://doi.org/10.1016/j.jhydrol.2016.05.020, 2016.

Kuang, X. and Jiao, J. J.: An integrated permeability-depth model for Earth's crust, 2, 7539–7545, https://doi.org/10.1002/2014GL061999.Received, 2014.

640 Laurent, A., Le Cozannet, G., Couëffé, R., Schroetter, J.-M., Croiset, N., and Lions, J.: Vulnérabilité des aquifères côtiers face aux intrusions salines en Normandie occidentale, Rapp. Final BRGM/RP-66052-FR, 189, 2017.

Lehner, B. and Grill, G.: Global river hydrography and network routing: Baseline data and new approaches to study the world's large river systems, Hydrol. Process., 27, 2171–2186, https://doi.org/10.1002/hyp.9740, 2013.

Lehner, B., Verdin, K., and Jarvis, A.: HydroSHEDS Technical Documentation Version 1.2, EOS Trans., 89, 26, 2013.

Leibowitz, S. G., Wigington, P. J., Schofield, K. A., Alexander, L. C., Vanderhoof, M. K., and Golden, H. E.: Connectivity of Streams and Wetlands to
645 Downstream Waters: An Integrated Systems Framework, J. Am. Water Resour. Assoc., 54, 298–322, https://doi.org/10.1111/1752-1688.12631, 2018.

Leray, S., de Dreuzy, J. R., Bour, O., Labasque, T., and Aquilina, L.: Contribution of age data to the characterization of complex aquifers, J. Hydrol., 464–465, 54–68, https://doi.org/10.1016/J.JHYDROL.2012.06.052, 2012.

Levizzani, V. and Cattani, E.: Satellite Remote Sensing of Precipitation and the Terrestrial Water Cycle in a Changing Climate, Remote Sens., 11, https://doi.org/10.3390/rs11192301, 2019.

650 Lindsay, J. B.: Whitebox GAT: A case study in geomorphometric analysis, Comput. Geosci., 95, 75–84, https://doi.org/10.1016/j.cageo.2016.07.003, 2016.

Linke, S., Lehner, B., Ouellet Dallaire, C., Ariwi, J., Grill, G., Anand, M., Beames, P., Burchard-Levine, V., Maxwell, S., Moidu, H., Tan, F., and Thieme, M.: Global hydro-environmental sub-basin and river reach characteristics at high spatial resolution, Sci. Data, 6, 1–16, https://doi.org/10.1038/s41597-019-0300-6, 2019.

Litwin, D. G., Tucker, G. E., Barnhart, K. R., and Harman, C. J.: Groundwater Affects the Geomorphic and Hydrologic Properties of Coevolved Landscapes,
655 J. Geophys. Res. Earth Surf., 127, 1–36, https://doi.org/10.1029/2021JF006239, 2022.

Lovill, S. M., Hahm, W. J., and Dietrich, W. E.: Drainage from the critical zone: lithologic controls on the persistence and spatial extent of wetted channels during the summer dry season, https://doi.org/10.1029/Water, 2018.

Luijendijk, E.: Transmissivity and groundwater flow exert a strong influence on drainage density, 1–32, 2021.

Luo, W. and Stepinski, T.: Identification of geologic contrasts from landscape dissection pattern: An application to the Cascade Range, Oregon, USA, 99, 90–
660 98, https://doi.org/10.1016/j.geomorph.2007.10.014, 2008.

Luo, W., Grudzinski, B. P., and Pederson, D.: Estimating hydraulic conductivity from drainage patterns-a case study in the Oregon Cascades, Geology, 38, 335–338, https://doi.org/10.1130/G30816.1, 2010.

Luo, W., Jasiewicz, J., Stepinski, T., Wang, J., Xu, C., and Cang, X.: Spatial association between dissection density and environmental factors over the entire conterminous United States, Geophys. Res. Lett., 43, 692–700, https://doi.org/10.1002/2015GL066941, 2016.

665 Marçais, J. and de Dreuzy, J. R.: Prospective Interest of Deep Learning for Hydrological Inference, 55, 688–692, https://doi.org/10.1111/gwat.12557, 2017.

Mardhel, V., Pinson, S., and Allier, D.: Description of an indirect method (IDPR) to determine spatial distribution of infiltration and runoff and its hydrogeological applications to the French territory, J. Hydrol., 592, https://doi.org/10.1016/j.jhydrol.2020.125609, 2021.

Mendoza, G. F., Steenhuis, T. S., Walter, M. T., and Parlange, J. Y.: Estimating basin-wide hydraulic parameters of a semi-arid mountainous watershed by recession-flow analysis, J. Hydrol., 279, 57–69, https://doi.org/10.1016/S0022-1694(03)00174-4, 2003.

670 Merot, P., Squividant, H., Aurousseau, P., Hefting, M., Burt, T., Maitre, V., Kruk, M., Butturini, A., Thenail, C., and Viaud, V.: Testing a climato-topographic index for predicting wetlands distribution along an European climate gradient, Ecol. Modell., 163, 51–71, https://doi.org/10.1016/S0304-3800(02)00387-3, 2003.

Messager, M. L., Lehner, B., Cockburn, C., Lamouroux, N., Pella, H., Snelder, T., Tockner, K., Trautmann, T., Watt, C., and Datry, T.: Global prevalence of non-perennial rivers and streams, Nature, 594, 391–397, https://doi.org/10.1038/s41586-021-03565-5, 2021.

675 Le Moigne, P., Besson, F., Martin, E., Boé, J., Decharme, B., Etchevers, P., Faroux, S., Habets, F., Lafaysse, M., Leroux, D., and Rousset-Regimbeau, F.: The Latest Improvements in SURFEX v8.0 of the Safran-Isba-Modcou Hydrometeorological Model over France, Geosci. Model Dev. Discuss., 1–32, https://doi.org/10.5194/gmd-2020-31, 2020.

Le Moine, N.: Le bassin versant de surface vu par le souterrain : une voie d'amélioration des performances et du réalisme des modèles pluie-débit ?, 348, 2008.

680 Mougin, B., Allier, D., Blanchin, R., Carn, A., Courtois, N., Gateau, C., and Putot, E.: SILURES Bretagne (Système d'Information pour la Localisation et l'Utilisation des Ressources en Eaux Souterraines), 2008.

Niswonger, R. G., Panday, S., and Ibaraki, M.: MODFLOW-NWT , A Newton Formulation for MODFLOW-2005, U.S. Geol. Surv. Tech. Methods, 6, 0–44,

2011.

Noilhan, J. and Mahfouf, J. F.: The ISBA land surface parameterisation scheme, Glob. Planet. Change, 13, 145–159, https://doi.org/10.1016/0921-8181(95)00043-7, 1996.

Pasquet, S., Marçais, J., Hayes, J. L., Sak, P. B., Ma, L., and Gaillardet, J.: Catchment-scale architecture of the deep critical zone revealed by seismic imaging, Geophys. Res. Lett., 1–13, https://doi.org/10.1029/2022gl098433, 2022.

Pederson, D. T.: Stream Piracy Revisited: A Groundwater-Sapping Solution, GSA Today, https://doi.org/10.1130/1052-5173(2001)011<0004:SPRAGS>2.0.CO;2, 2001.

Pelletier, J. D., Broxton, P. D., Hazenberg, P., Zeng, X., Troch, P. A., Niu, G. Y., Williams, Z., Brunke, M. A., and Gochis, D.: A gridded global data set of soil, intact regolith, and sedimentary deposit thicknesses for regional and global land surface modeling, J. Adv. Model. Earth Syst., 8, 41–65, https://doi.org/10.1002/2015MS000526, 2016.

Prancevic, J. P. and Kirchner, J. W.: Topographic Controls on the Extension and Retraction of Flowing Streams, Geophys. Res. Lett., 46, 2084–2092, https://doi.org/10.1029/2018GL081799, 2019.

Quintana-Seguí, P., Le Moigne, P., Durand, Y., Martin, E., Habets, F., Baillon, M., Canellas, C., Franchisteguy, L., and Morel, S.: Analysis of near-surface atmospheric variables: Validation of the SAFRAN analysis over France, J. Appl. Meteorol. Climatol., 47, 92–107, https://doi.org/10.1175/2007JAMC1636.1, 2008.

Ranjram, M., Gleeson, T., and Luijendijk, E.: Is the permeability of crystalline rock in the shallow crust related to depth, lithology or tectonic setting?, 15, 106–119, https://doi.org/https://doi.org/10.1111/gfl.12098, 2015.

Rapinel, S., Panhelleux, L., Gayet, G., Vanacker, R., Lemercier, B., Laroche, B., Chambaud, F., Guelmami, A., and Hubert-Moy, L.: National wetland mapping using remote-sensing-derived environmental variables, archive field data, and artificial intelligence, 9, 1–17, https://doi.org/10.1016/j.heliyon.2023.e13482, 2023.

Refsgaard, J. C., Hojberg, A. L., Moller, I., Hansen, M., and Sondergaard, V.: Groundwater modeling in integrated water resources management--visions for 2020, Ground Water, 48, 633–648, https://doi.org/10.1111/j.1745-6584.2009.00634.x, 2010.

Reichstein, M., Camps-Valls, G., Stevens, B., Jung, M., Denzler, J., Carvalhais, N., and Prabhat: Deep learning and process understanding for data-driven Earth system science, Nature, 566, 195–204, 2019.

Renard, P.: The future of hydraulic tests, Hydrogeol. J., 13, 259–262, https://doi.org/10.1007/s10040-004-0406-5, 2005.

Roques, C., Aquilina, L., Bour, O., Maréchal, J. C., Dewandel, B., Pauwels, H., Labasque, T., Vergnaud-Ayraud, V., and Hochreutener, R.: Groundwater sources and geochemical processes in a crystalline fault aquifer, J. Hydrol., 519, 3110–3128, https://doi.org/10.1016/j.jhydrol.2014.10.052, 2014.

Roques, C., Bour, O., Aquilina, L., and Dewandel, B.: High-yielding aquifers in crystalline basement: insights about the role of fault zones, exemplified by Armorican Massif, France, Hydrogeol. J., 24, 2157–2170, https://doi.org/10.1007/s10040-016-1451-6, 2016.

Rotzoll, K. and El-Kadi, A. I.: Estimating hydraulic properties of coastal aquifers using wave setup, J. Hydrol., 353, 201–213, https://doi.org/10.1016/j.jhydrol.2008.02.005, 2008.

Schilling, O. S., Cook, P. G., and Brunner, P.: Beyond Classical Observations in Hydrogeology: The Advantages of Including Exchange Flux, Temperature, Tracer Concentration, Residence Time, and Soil Moisture Observations in Groundwater Model Calibration, Rev. Geophys., 57, 146–182, https://doi.org/10.1029/2018RG000619, 2019.

Schneider, A., Jost, A., Coulon, C., Silvestre, M., Théry, S., and Ducharne, A.: Global-scale river network extraction based on high-resolution topography and constrained by lithology, climate, slope, and observed drainage density, Geophys. Res. Lett., 44, 2773–2781, https://doi.org/10.1002/2016GL071844, 2017.

Schumm, S. A., Boyd, K. F., Wolff, C. G., and Spitz, W. J.: A ground-water sapping landscape in the Florida Panhandle, 12, 281–297, 1995.

Shangguan, W., Hengl, T., Mendes de Jesus, J., Yuan, H., and Dai, Y.: Mapping the global depth to bedrock for land surface modeling, J. Adv. Model. Earth Syst., 9, 65–88, https://doi.org/10.1002/2016MS000686, 2017.

Sivapalan, M., Takeuchi, K., Franks, S. W., Gupta, V. K., Karambiri, H., Lakshmi, V., Liang, X., McDonnell, J. J., Mendiondo, E. M., O'Connell, P. E., Oki, T., Pomeroy, J. W., Schertzer, D., Uhlenbrook, S., and Zehe, E.: IAHS Decade on Predictions in Ungauged Basins (PUB), 2003-2012: Shaping an exciting future for the hydrological sciences, Hydrol. Sci. J., 48, 857–880, https://doi.org/10.1623/hysj.48.6.857.51421, 2003.

Sophocleous, M.: Interactions between groundwater and surface water: the state of the science, Hydrogeol. J., 10, 52–67, https://doi.org/10.1007/s10040-001-0170-8, 2002.

Stoll, S. and Weiler, M.: Explicit simulations of stream networks to guide hydrological modelling in ungauged basins, Hydrol. Earth Syst. Sci., 14, 1435–1448, https://doi.org/10.5194/hess-14-1435-2010, 2010.

Strahler, A. N.: Quantitative geomorphology of drainage basins and channel networks, Chow, V.T. Handb. Appl. Hydrol. McGraw-Hill, New York, 439–476, 1964.

Tashie, A., Pavelsky, T. M., Band, L., and Topp, S.: Watershed-Scale Effective Hydraulic Properties of the Continental United States Journal of Advances in Modeling Earth Systems, 1–18, https://doi.org/10.1029/2020MS002440, 2021.

Taylor, R. G., Scanlon, B., Doll, P., Rodell, M., van Beek, R., Wada, Y., Longuevergne, L., Leblanc, M., Famiglietti, J. S., Edmunds, M., Konikow, L., Green, T. R., Chen, J. Y., Taniguchi, M., Bierkens, M. F. P., MacDonald, A., Fan, Y., Maxwell, R. M., Yechieli, Y., Gurdak, J. J., Allen, D. M., Shamsudduha, M., Hiscock, K., Yeh, P. J. F., Holman, I., and Treidel, H.: Ground water and climate change, Nat. Clim. Chang., 3, 322–329, https://doi.org/10.1038/nclimate1744, 2013.

Tootchi, A., Jost, A., and Ducharne, A.: Multi-source global wetland maps combining surface water imagery and groundwater constraints, Earth Syst. Sci. Data, 11, 189–220, https://doi.org/10.5194/essd-11-189-2019, 2019.

Troch, P. A., Berne, A., Bogaart, P., Harman, C., Hilberts, A. G. J., Lyon, S. W., Paniconi, C., Pauwels, V. R. N., Rupp, D. E., Selker, J. S., Teuling, A. J., Uijlenhoet, R., and Verhoest, N. E. C.: The importance of hydraulic groundwater theory in catchment hydrology: The legacy of Wilfried Brutsaert and Jean-Yves Parlange, Water Resour. Res., 49, 5099–5116, https://doi.org/10.1002/wrcr.20407, 2013.

Vannier, O., Braud, I., and Anquetin, S.: Regional estimation of catchment-scale soil properties by means of streamflow recession analysis for use in distributed hydrological models, Hydrol. Process., 28, 6276–6291, https://doi.org/10.1002/hyp.10101, 2014.

Vautier, C., Abhervé, R., Labasque, T., Laverman, A. M., Guillou, A., Chatton, E., Dupont, P., Aquilina, L., and de Dreuzy, J.-R.: Mapping gas exchanges in headwater streams with membrane inlet mass spectrometry, J. Hydrol., https://doi.org/10.1016/j.jhydrol.2019.124398, 2019.

Vergnes, J.-P., Roux, N., Habets, F., Ackerer, P., Amraoui, N., Besson, F., Caballero, Y., Courtois, Q., de Dreuzy, J.-R., Etchevers, P., Gallois, N., Leroux, D. J., Longuevergne, L., Le Moigne, P., Morel, T., Munier, S., Regimbeau, F., Thiéry, D., and Viennot, P.: The AquiFR hydrometeorological modelling platform as a tool for improving groundwater resource monitoring over France: evaluation over a 60-year period, Hydrol. Earth Syst. Sci., 24, 633–654, https://doi.org/10.5194/hess-24-633-2020, 2020.

Vergopolan, N., Chaney, N. W., Pan, M., Sheffield, J., Beck, H. E., Ferguson, C. R., Torres-Rojas, L., Sadri, S., and Wood, E. F.: SMAP-HydroBlocks, a 30-m satellite-based soil moisture dataset for the conterminous US, Sci. Data, 8, 1–11, https://doi.org/10.1038/s41597-021-01050-2, 2021.

Vidal, J. P., Martin, E., Franchistéguy, L., Baillon, M., and Soubeyroux, J. M.: A 50-year high-resolution atmospheric reanalysis over France with the Safran system, Int. J. Climatol., 30, 1627–1644, https://doi.org/10.1002/joc.2003, 2010.

Vries, J. J. De: Dynamics of the interface between streams and groundwater systems in lowland areas, with reference to stream net evolution, J. Hydrol., 1694, 1994.

Wada, Y., van Beek, L. P. H., van Kempen, C. M., Reckman, J., Vasak, S., and Bierkens, M. F. P.: Global depletion of groundwater resources, Geophys. Res. Lett., 37, https://doi.org/10.1029/2010gl044571, 2010.

Warix, S. R., Godsey, S. E., Lohse, K. A., and Hale, R. L.: Influence of groundwater and topography on stream drying in semi-arid headwater streams, Hydrol. Process., 35, 1–18, https://doi.org/10.1002/hyp.14185, 2021.

Weiler, M. and McDonnell, J.: Virtual experiments: A new approach for improving process conceptualization in hillslope hydrology, J. Hydrol., 285, 3–18, https://doi.org/10.1016/S0022-1694(03)00271-3, 2004.

Whiting, J. A. and Godsey, S. E.: Discontinuous headwater stream networks with stable flowheads, Salmon River basin, Idaho, Hydrol. Process., 30, 2305–2316, https://doi.org/10.1002/hyp.10790, 2016.

Wigmosta, M. S. and Lettenmaier, P.: A comparison of simplified methods for routing topographically driven subsurface flow, Water Resour., 35, 255–264, 1999.

Winter, T. C.: Relation of streams, lakes, and wetlands to groundwater flow systems, Hydrogeol. J., 7, 28–45, https://doi.org/10.1007/s100400050178, 1999.

Yamazaki, D., Ikeshima, D., Tawatari, R., Yamaguchi, T., O'Loughlin, F., Neal, J. C., Sampson, C. C., Kanae, S., and Bates, P. D.: A high-accuracy map of global terrain elevations, Geophys. Res. Lett., 44, 5844–5853, https://doi.org/10.1002/2017GL072874, 2017.

Yamazaki, D., Ikeshima, D., Sosa, J., Bates, P. D., Allen, G. H., and Pavelsky, T. M.: MERIT Hydro: A High-Resolution Global Hydrography Map Based on Latest Topography Dataset, Water Resour. Res., 55, 5053–5073, https://doi.org/10.1029/2019WR024873, 2019.

Yoshida, T. and Troch, P. A.: Coevolution of volcanic catchments in Japan, Hydrol. Earth Syst. Sci., 20, 1133–1150, https://doi.org/10.5194/hess-20-1133-2016, 2016.

Zlotnik, V. A. and Zurbuchen, B. R.: Estimation of hydraulic conductivity from borehole flowmeter tests considering head losses, J. Hydrol., 281, 115–128, https://doi.org/10.1016/S0022-1694(03)00204-X, 2003.